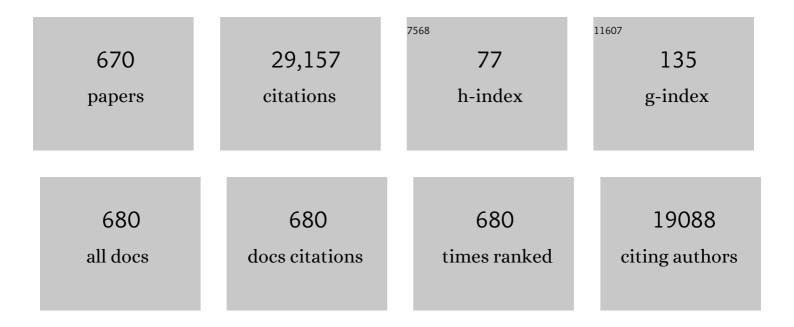
List of Publications by Year in descending order

Source: https://exaly.com/author-pdf/5333061/publications.pdf Version: 2024-02-01



HAL-YAN MANC

#	Article	IF	CITATIONS
1	Highly anisotropic and robust excitons in monolayer black phosphorus. Nature Nanotechnology, 2015, 10, 517-521.	31.5	1,204
2	Strongly enhanced current densities in superconducting coated conductors of YBa2Cu3O7–x + BaZrO3. Nature Materials, 2004, 3, 439-443.	27.5	1,118
3	Materials science challenges for high-temperature superconducting wire. Nature Materials, 2007, 6, 631-642.	27.5	670
4	Stainless steel as bipolar plate material for polymer electrolyte membrane fuel cells. Journal of Power Sources, 2003, 115, 243-251.	7.8	606
5	Deformation behavior and plastic instabilities of ultrafine-grained titanium. Applied Physics Letters, 2001, 79, 611-613.	3.3	413
6	Strain control and spontaneous phase ordering in vertical nanocomposite heteroepitaxial thin films. Nature Materials, 2008, 7, 314-320.	27.5	334
7	A ferroelectric semiconductor field-effect transistor. Nature Electronics, 2019, 2, 580-586.	26.0	317
8	Polymer-assisted deposition of metal-oxide films. Nature Materials, 2004, 3, 529-532.	27.5	308
9	Radiation damage in nanostructured materials. Progress in Materials Science, 2018, 96, 217-321.	32.8	307
10	Strain hardening and large tensile elongation in ultrahigh-strength nano-twinned copper. Applied Physics Letters, 2004, 85, 4932-4934.	3.3	304
11	Giant optical anisotropy in a quasi-one-dimensional crystal. Nature Photonics, 2018, 12, 392-396.	31.4	269
12	Enhanced hardening in Cu/330 stainless steel multilayers by nanoscale twinning. Acta Materialia, 2004, 52, 995-1002.	7.9	263
13	Enhanced tensile ductility and toughness in nanostructured Cu. Applied Physics Letters, 2002, 80, 2395-2397.	3.3	254
14	Angular-dependent vortex pinning mechanisms in YBa2Cu3O7 coated conductors and thin films. Applied Physics Letters, 2004, 84, 2121-2123.	3.3	254
15	Thermal stability of sputtered Cu films with nanoscale growth twins. Journal of Applied Physics, 2008, 103, .	2.5	231
16	Thick lead-free ferroelectric films with high Curie temperatures through nanocomposite-induced strain. Nature Nanotechnology, 2011, 6, 491-495.	31.5	220
17	Nanoscale-twinning-induced strengthening in austenitic stainless steel thin films. Applied Physics Letters, 2004, 84, 1096-1098.	3.3	217
18	High-strength sputter-deposited Cu foils with preferred orientation of nanoscale growth twins. Applied Physics Letters, 2006, 88, 173116.	3.3	209

#	Article	IF	CITATIONS
19	Mechanical properties of highly textured Cu/Ni multilayers. Acta Materialia, 2011, 59, 1924-1933.	7.9	202
20	Epitaxial nanotwinned Cu films with high strength and high conductivity. Applied Physics Letters, 2008, 93, .	3.3	192
21	Interface enabled defects reduction in helium ion irradiated Cu/V nanolayers. Journal of Nuclear Materials, 2010, 407, 178-188.	2.7	189
22	Controlled Growth of a Large-Size 2D Selenium Nanosheet and Its Electronic and Optoelectronic Applications. ACS Nano, 2017, 11, 10222-10229.	14.6	189
23	Overcoming the barrier to 1000Aâ^•cm width superconducting coatings. Applied Physics Letters, 2005, 87, 162505.	3.3	182
24	He ion irradiation damage in Fe/W nanolayer films. Journal of Nuclear Materials, 2009, 389, 233-238.	2.7	179
25	Temperature and strain rate effects on the strength and ductility of nanostructured copper. Applied Physics Letters, 2003, 83, 3165-3167.	3.3	176
26	Rectifying current-voltage characteristics of BiFeO3â^•Nb-doped SrTiO3 heterojunction. Applied Physics Letters, 2008, 92, .	3.3	176
27	Reviewing Metallic PEMFC Bipolar Plates. Fuel Cells, 2010, 10, 510-519.	2.4	176
28	Tunable Lowâ€Field Magnetoresistance in (La <sub>0.7</sub> Sr <sub>0.3</sub> MnO <sub>3</sub> ) <sub>0.5</sub> :(ZnO) <sub>0.5</sub> Selfâ€Assembled Vertically Aligned Nanocomposite Thin Films. Advanced Functional Materials, 2011, 21, 2423-2429.	14.9	174
29	Structural, electrical, and terahertz transmission properties of VO2 thin films grown on c-, r-, and m-plane sapphire substrates. Journal of Applied Physics, 2012, 111, .	2.5	172
30	Preferential thermal nitridation to form pin-hole free Cr-nitrides to protect proton exchange membrane fuel cell metallic bipolar plates. Scripta Materialia, 2004, 50, 1017-1022.	5.2	168
31	Removal of stacking-fault tetrahedra by twin boundaries in nanotwinned metals. Nature Communications, 2013, 4, 1377.	12.8	155
32	Radiation damage in helium ion irradiated nanocrystalline Fe. Journal of Nuclear Materials, 2012, 425, 140-146.	2.7	154
33	Microstructure, vertical strain control and tunable functionalities in self-assembled, vertically aligned nanocomposite thin films. Acta Materialia, 2013, 61, 2783-2792.	7.9	153
34	Mechanical properties of sputtered Cu/V and Al/Nb multilayer films. Materials Science & Engineering A: Structural Materials: Properties, Microstructure and Processing, 2008, 493, 283-287.	5.6	145
35	Strongly enhanced oxygen ion transport through samarium-doped CeO2 nanopillars in nanocomposite films. Nature Communications, 2015, 6, 8588.	12.8	145
36	High strength, epitaxial nanotwinned Ag films. Acta Materialia, 2011, 59, 93-101.	7.9	144

#	Article	IF	CITATIONS
37	Thermally nitrided stainless steels for polymer electrolyte membrane fuel cell bipolar plates. Journal of Power Sources, 2004, 138, 79-85.	7.8	142
38	On the origin of ultrahigh cryogenic strength of nanocrystalline metals. Applied Physics Letters, 2004, 85, 2750-2752.	3.3	136
39	Systematic enhancement of in-field critical current density with rare-earth ion size variance in superconducting rare-earth barium cuprate films. Applied Physics Letters, 2004, 84, 5329-5331.	3.3	127
40	Raman response and transport properties of tellurium atomic chains encapsulated in nanotubes. Nature Electronics, 2020, 3, 141-147.	26.0	126
41	Nanostructured Cu/Nb multilayers subjected to helium ion-irradiation. Nuclear Instruments & Methods in Physics Research B, 2007, 261, 1129-1132.	1.4	125
42	Oxygen concentration and its effect on the leakage current in BiFeO3 thin films. Applied Physics Letters, 2010, 96, .	3.3	124
43	Thermally nitrided stainless steels for polymer electrolyte membrane fuel cell bipolar plates. Journal of Power Sources, 2004, 138, 86-93.	7.8	120
44	Strongly coupled critical current density values achieved in Y1Ba2Cu3O7â^'δ coated conductors with near-single-crystal texture. Applied Physics Letters, 2003, 82, 4519-4521.	3.3	115
45	Studies of deformation mechanisms in ultra-fine-grained and nanostructured Zn. Acta Materialia, 2002, 50, 4823-4830.	7.9	113
46	Self-assembled, rare earth tantalate pyrochlore nanoparticles for superior flux pinning in YBa <sub>2</sub> Cu <sub>3</sub> O <sub>7â^î´</sub> films. Superconductor Science and Technology, 2009, 22, 022001.	3.5	109
47	Stacking fault and partial dislocation dominated strengthening mechanisms in highly textured Cu/Co multilayers. International Journal of Plasticity, 2013, 49, 152-163.	8.8	109
48	In situ nanoindentation study on plasticity and work hardening in aluminium with incoherent twin boundaries. Nature Communications, 2014, 5, 4864.	12.8	107
49	Size dependent enhancement of helium ion irradiation tolerance in sputtered Cu/V nanolaminates. Journal of Nuclear Materials, 2009, 385, 629-632.	2.7	104
50	Microstructure and strengthening mechanisms in Cu/Fe multilayers. Acta Materialia, 2012, 60, 6312-6321.	7.9	104
51	ldentification of Intrinsic ab-Plane Pinning in <tex>\$rm YBa_2rm Cu_3rm O_7\$</tex> Thin Films and Coated Conductors. IEEE Transactions on Applied Superconductivity, 2005, 15, 2808-2811.	1.7	103
52	In situ Evidence of Defect Cluster Absorption by Grain Boundaries in Kr Ion Irradiated Nanocrystalline Ni. Metallurgical and Materials Transactions A: Physical Metallurgy and Materials Science, 2013, 44, 1966-1974.	2.2	103
53	Vertically Aligned Nanocomposite Thin Films as a Cathode/Electrolyte Interface Layer for Thinâ€Film Solid Oxide Fuel Cells. Advanced Functional Materials, 2009, 19, 3868-3873.	14.9	101
54	Why In <sub>2</sub> O <sub>3</sub> Can Make 0.7 nm Atomic Layer Thin Transistors. Nano Letters, 2021, 21, 500-506.	9.1	99

#	Article	IF	CITATIONS
55	Interfacial coupling in heteroepitaxial vertically aligned nanocomposite thin films: From lateral to vertical control. Current Opinion in Solid State and Materials Science, 2014, 18, 6-18.	11.5	98
56	Scaled indium oxide transistors fabricated using atomic layer deposition. Nature Electronics, 2022, 5, 164-170.	26.0	98
57	Nanotwins and stacking faults in high-strength epitaxial Ag/Al multilayer films. Applied Physics Letters, 2012, 101, .	3.3	97
58	Damage-tolerant nanotwinned metals with nanovoids under radiation environments. Nature Communications, 2015, 6, 7036.	12.8	97
59	High‣trength Nanotwinned Al Alloys with 9R Phase. Advanced Materials, 2018, 30, 1704629.	21.0	93
60	High power density thin film SOFCs with YSZ/GDC bilayer electrolyte. Electrochimica Acta, 2011, 56, 5472-5477.	5.2	92
61	Interface lattice displacement measurement to 1pm by geometric phase analysis on aberration-corrected HAADF STEM images. Acta Materialia, 2013, 61, 5646-5663.	7.9	91
62	Self-Assembled Epitaxial Au–Oxide Vertically Aligned Nanocomposites for Nanoscale Metamaterials. Nano Letters, 2016, 16, 3936-3943.	9.1	91
63	In Situ Study of Defect Migration Kinetics and Self-Healing of Twin Boundaries in Heavy Ion Irradiated Nanotwinned Metals. Nano Letters, 2015, 15, 2922-2927.	9.1	90
64	lonic Conductivity Increased by Two Orders of Magnitude in Micrometer-Thick Vertical Yttria-Stabilized ZrO <sub>2</sub> Nanocomposite Films. Nano Letters, 2015, 15, 7362-7369.	9.1	90
65	Strong oxygen pressure dependence of ferroelectricity in BaTiO3/SrRuO3/SrTiO3 epitaxial heterostructures. Journal of Applied Physics, 2013, 114, .	2.5	88
66	Vertical Interface Effect on the Physical Properties of Selfâ€Assembled Nanocomposite Epitaxial Films. Advanced Materials, 2009, 21, 3794-3798.	21.0	87
67	Continuous Tuning of Phase Transition Temperature in VO <sub>2</sub> Thin Films on <i>c</i> Cut Sapphire Substrates via Strain Variation. ACS Applied Materials & Interfaces, 2017, 9, 5319-5327.	8.0	87
68	High temperature deformability of ductile flash-sintered ceramics via in-situ compression. Nature Communications, 2018, 9, 2063.	12.8	87
69	Thick YBa2Cu3O7â^'x+BaSnO3 films with enhanced critical current density at high magnetic fields. Applied Physics Letters, 2008, 93, .	3.3	86
70	New epitaxy paradigm in epitaxial self-assembled oxide vertically aligned nanocomposite thin films. Journal of Materials Research, 2017, 32, 4054-4066.	2.6	86
71	Evidence for the formation mechanism of nanoscale microstructures in cryomilled Zn powder. Acta Materialia, 2001, 49, 1319-1326.	7.9	85
72	Understanding High Critical Currents in YBa2Cu3O7Thin Films and Coated Conductors. Journal of Low Temperature Physics, 2004, 135, 87-98.	1.4	84

#	Article	IF	CITATIONS
73	Superior radiation-resistant nanoengineered austenitic 304L stainless steel for applications in extreme radiation environments. Scientific Reports, 2015, 5, 7801.	3.3	82
74	Nanoscale stacking fault–assisted room temperature plasticity in flash-sintered TiO <sub>2</sub> . Science Advances, 2019, 5, eaaw5519.	10.3	82
75	Self-assembled oxide films with tailored nanoscale ionic and electronic channels for controlled resistive switching. Nature Communications, 2016, 7, 12373.	12.8	81
76	Formation Mechanisms of High-density Growth Twins in Aluminum with High Stacking-Fault Energy. Materials Research Letters, 2013, 1, 51-60.	8.7	80
77	In situ Nanoindentation Study of Plastic Co-deformation in Al-TiN Nanocomposites. Scientific Reports, 2014, 4, 6633.	3.3	80
78	Role of scaffold network in controlling strain and functionalities of nanocomposite films. Science Advances, 2016, 2, e1600245.	10.3	80
79	Surface Functionalization of Layered Molybdenum Disulfide for the Selective Detection of Volatile Organic Compounds at Room Temperature. ACS Applied Materials & Interfaces, 2019, 11, 34135-34143.	8.0	79
80	Enhanced radiation tolerance of ultrafine grained Fe–Cr–Ni alloy. Journal of Nuclear Materials, 2012, 420, 235-240.	2.7	78
81	A New Class of Roomâ€Temperature Multiferroic Thin Films with Bismuthâ€Based Supercell Structure. Advanced Materials, 2013, 25, 1028-1032.	21.0	78
82	He ion irradiation damage in Alâ^•Nb multilayers. Journal of Applied Physics, 2009, 105, .	2.5	77
83	Ultrafast measurements of polarization switching dynamics on ferroelectric and anti-ferroelectric hafnium zirconium oxide. Applied Physics Letters, 2019, 115, .	3.3	77
84	Influence of crystalline texture on vortex pinning near the ab-plane in YBa2Cu3O7 thin films and coated conductors. Physica C: Superconductivity and Its Applications, 2004, 412-414, 976-982.	1.2	76
85	A roadmap for tailoring the strength and ductility of ferritic/martensitic T91 steel via thermo-mechanical treatment. Acta Materialia, 2016, 112, 361-377.	7.9	76
86	VO 2 multidomain heteroepitaxial growth and terahertz transmission modulation. Applied Physics Letters, 2010, 97, .	3.3	75
87	Novel Electroformingâ€Free Nanoscaffold Memristor with Very High Uniformity, Tunability, and Density. Advanced Materials, 2014, 26, 6284-6289.	21.0	75
88	Unusual size-dependent strengthening mechanisms in helium ion-irradiated immiscible coherent Cu/Co nanolayers. Acta Materialia, 2015, 84, 393-404.	7.9	75
89	In-situ observation of oxygen mobility and abnormal lattice expansion in ceria during flash sintering. Ceramics International, 2018, 44, 15362-15369.	4.8	75
90	Tensile elongation (110%) observed in ultrafine-grained Zn at room temperature. Applied Physics Letters, 2002, 81, 823-825.	3.3	72

#	Article	IF	CITATIONS
91	In situ studies of irradiation-induced twin boundary migration in nanotwinned Ag. Scripta Materialia, 2013, 69, 385-388.	5.2	72
92	Superior corrosion resistance properties of TiN-based coatings on Zircaloy tubes in supercritical water. Journal of Nuclear Materials, 2014, 451, 346-351.	2.7	71
93	Microstructure, magnetic, and low-field magnetotransport properties of self-assembled (La <sub>0.7</sub> Sr <sub>0.3</sub> MnO <sub>3</sub> ) <sub>0.5</sub> :(CeO <sub>2</sub> ) <sub>0.5</sub> aligned nanocomposite thin films. Nanotechnology, 2011, 22, 315712.	ver <b>zic</b> ally	70
94	Multifunctional, self-assembled oxide nanocomposite thin films and devices. MRS Bulletin, 2015, 40, 736-745.	3.5	70
95	Mechanical behavior of structurally gradient nickel alloy. Acta Materialia, 2018, 149, 57-67.	7.9	70
96	Ion irradiation effects in nanocrystalline TiN coatings. Nuclear Instruments & Methods in Physics Research B, 2007, 261, 1162-1166.	1.4	69
97	Growth of â^1⁄45 cm2Vâ^'1sâ^'1 mobility, p-type Copper(I) oxide (Cu2O) films by fast atmospheric atomic layer deposition (AALD) at 225°C and below. AIP Advances, 2012, 2, .	1.3	69
98	Extremely High Tunability and Low Loss in Nanoscaffold Ferroelectric Films. Nano Letters, 2012, 12, 4311-4317.	9.1	69
99	Room-Temperature Electrocaloric Effect in Layered Ferroelectric CuInP <sub>2</sub> S <sub>6</sub> for Solid-State Refrigeration. ACS Nano, 2019, 13, 8760-8765.	14.6	69
100	The influence of interfaces on the formation of bubbles in He-ion-irradiated Cu/Mo nanolayers. Philosophical Magazine Letters, 2011, 91, 18-28.	1.2	68
101	Comparisons of radiation damage in He ion and proton irradiated immiscible Ag/Ni nanolayers. Journal of Nuclear Materials, 2013, 440, 310-318.	2.7	68
102	Enhancement and angular dependence of transport critical current density in pulsed laser deposited YBa2Cu3O7â^'x+BaSnO3 films in applied magnetic fields. Journal of Applied Physics, 2007, 102, .	2.5	67
103	How (Ba <sub>0.5</sub> Sr <sub>0.5</sub> )(Fe <sub>0.8</sub> Zn <sub>0.2</sub> )O <sub>3–Î</sub> and (Ba <sub>0.5</sub> Sr <sub>0.5</sub> )(Co <sub>0.8</sub> Fe <sub>0.2</sub> )O <sub>3–Î</sub> Perovskites Form via an EDTA/Citric Acid Complexing Method. Advanced Materials, 2007, 19, 2134-2140.	21.0	67
104	In situ study of defect migration kinetics in nanoporous Ag with enhanced radiation tolerance. Scientific Reports, 2014, 4, 3737.	3.3	67
105	Green luminescent zinc oxide films prepared by polymer-assisted deposition with rapid thermal process. Thin Solid Films, 2005, 492, 101-104.	1.8	66
106	Effects of deposition parameters on residual stresses, hardness and electrical resistivity of nanoscale twinned 330 stainless steel thin films. Journal of Applied Physics, 2005, 97, 094302.	2.5	66
107	Response of nanocrystalline <mml:math <br="" xmlns:mml="http://www.w3.org/1998/Math/MathML">display="inline"&gt;<mml:mrow><mml:mn>3</mml:mn><mml:mi>C</mml:mi></mml:mrow></mml:math> silicon carbide to heavy-ion irradiation. Physical Review B, 2009, 80, .	3.2	66
108	Direct observation of Lomer-Cottrell Locks during strain hardening in nanocrystalline nickel by in situ TEM. Scientific Reports, 2013, 3, 1061.	3.3	66

#	Article	IF	CITATIONS
109	High-velocity projectile impact induced 9R phase in ultrafine-grained aluminium. Nature Communications, 2017, 8, 1653.	12.8	66
110	Intrinsic ferroelectricity in Y-doped HfO2 thin films. Nature Materials, 2022, 21, 903-909.	27.5	66
111	Rare earth ion size effects and enhanced critical current densities in Y2â^•3Sm1â^•3Ba2Cu3O7â^'x coated conductors. Applied Physics Letters, 2005, 86, 032505.	3.3	65
112	The role of point defects and defect gradients in flash sintering of perovskite oxides. Acta Materialia, 2019, 165, 398-408.	7.9	65
113	Low field magnetotransport properties of (La0.7Sr0.3MnO3)0.5:(ZnO)0.5 nanocomposite films. Applied Physics Letters, 2006, 88, 192514.	3.3	64
114	Leakage mechanisms of self-assembled (BiFeO3)0.5:(Sm2O3)0.5 nanocomposite films. Applied Physics Letters, 2008, 93, .	3.3	64
115	State-of-the-art flux pinning in YBa <sub>2</sub> Cu <sub>3</sub> O <sub>7 a T</sub> by the creation of highly linear, segmented nanorods of Ba <sub>2</sub> (Y /Gd)(Nb/Ta)O <sub>6</sub> together with nanoparticles of (Y /Gd) <sub>2</sub> O <sub>3</sub> and (Y) Tj ETQq1 1 0.784314 rgBT /Overlock 10 Tf 50 497	7 <b>⊺cå.(</b> ∮Gd)।	3a≺ <b>s</b> ∙ub>2
116	095012. Self-assembled Co–BaZrO <sub>3</sub> nanocomposite thin films with ultra-fine vertically aligned Co nanopillars. Nanoscale, 2017, 9, 7970-7976.	5.6	64
117	Structural and dielectric properties of epitaxial Ba1â <sup>~°</sup> xSrxTiO3 films grown on LaAlO3 substrates by polymer-assisted deposition. Applied Physics Letters, 2004, 85, 5007-5009.	3.3	63
118	In situ studies on radiation tolerance of nanotwinned Cu. Acta Materialia, 2016, 111, 148-156.	7.9	63
119	The formation of protective nitride surfaces for PEM fuel cell metallic bipolar plates. Jom, 2006, 58, 50-57.	1.9	62
120	Multifunctional La <sub>0.67</sub> Sr <sub>0.33</sub> MnO <sub>3</sub> (LSMO) Thin Films Integrated on Mica Substrates toward Flexible Spintronics and Electronics. ACS Applied Materials & Interfaces, 2018, 10, 42698-42705.	8.0	62
121	High critical current YBCO coated conductors based on IBAD MgO. Physica C: Superconductivity and Its Applications, 2004, 412-414, 795-800.	1.2	61
122	Application of weak ferromagnetic BiFeO3 films as the photoelectrode material under visible-light irradiation. Applied Physics Letters, 2007, 91, .	3.3	61
123	Unusual size dependent strengthening mechanisms of Cu/amorphous CuNb multilayers. Acta Materialia, 2016, 120, 327-336.	7.9	61
124	Inhomogeneous reduction and its relation to grain growth of titania during flash sintering. Scripta Materialia, 2018, 155, 37-40.	5.2	60
125	Induced Magnetization in <mml:math <br="" xmlns:mml="http://www.w3.org/1998/Math/MathML">display="inline"&gt;<mml:mrow><mml:msub><mml:mrow><mml:mi>La</mml:mi></mml:mrow><mml:mrow><mm Physical Review Letters, 2014, 113, 047204.</mm </mml:mrow></mml:msub></mml:mrow></mml:math>	l:m <b>7</b> 380.7<	/m <b>59:</b> mn> </td
126	Ultra-smooth glassy graphene thin films for flexible transparent circuits. Science Advances, 2016, 2, e1601574.	10.3	59

#	Article	IF	CITATIONS
127	Integration of Self-Assembled Vertically Aligned Nanocomposite (La <sub>0.7</sub> Sr <sub>0.3</sub> MnO <sub>3</sub> 1– <i>x</i> :(ZnO) <sub><i>x</i></sub> Thin Films on Silicon Substrates. ACS Applied Materials & Interfaces, 2013, 5, 3995-3999.	8.0	58
128	Three-dimensional strain engineering in epitaxial vertically aligned nanocomposite thin films with tunable magnetotransport properties. Materials Horizons, 2018, 5, 536-544.	12.2	57
129	An Electronic Synapse Based on 2D Ferroelectric CuInP <sub>2</sub> S <sub>6</sub> . Advanced Electronic Materials, 2020, 6, 2000760.	5.1	57
130	Comparison of size dependent strengthening mechanisms in Ag/Fe and Ag/Ni multilayers. Acta Materialia, 2016, 114, 154-163.	7.9	56
131	Nanoscale Artificial Plasmonic Lattice in Selfâ€Assembled Vertically Aligned Nitride–Metal Hybrid Metamaterials. Advanced Science, 2018, 5, 1800416.	11.2	56
132	Size dependent strengthening in high strength nanotwinned Al/Ti multilayers. Acta Materialia, 2019, 175, 466-476.	7.9	56
133	Selfâ€Assembled Ordered Threeâ€Phase Au–BaTiO <sub>3</sub> –ZnO Vertically Aligned Nanocomposites Achieved by a Templating Method. Advanced Materials, 2019, 31, e1806529.	21.0	56
134	Significant enhancement of the strength-to-resistivity ratio by nanotwins in epitaxial Cu films. Journal of Applied Physics, 2009, 106, .	2.5	55
135	Influence of naturally grown nanoparticles at the buffer layer in the flux pinning in YBa2Cu3O7coated conductors. Superconductor Science and Technology, 2006, 19, 891-895.	3.5	54
136	P-type ZnO thin films achieved by N+ ion implantation through dynamic annealing process. Applied Physics Letters, 2012, 101, .	3.3	54
137	Strain Tuning and Strong Enhancement of Ionic Conductivity in SrZrO <sub>3</sub> –RE <sub>2</sub> O <sub>3</sub> (RE = Sm, Eu, Gd, Dy, and Er) Nanocomposite Films. Advanced Functional Materials, 2015, 25, 4328-4333.	14.9	54
138	Controlling Oxidation States in Uranium Oxides through Epitaxial Stabilization. Advanced Materials, 2007, 19, 3559-3563.	21.0	53
139	Electrochemical Properties of Nanocrystalline La <sub>0.5</sub> Sr <sub>0.5</sub> CoO <sub>3â^'<i>x</i></sub> Thin Films. Chemistry of Materials, 2010, 22, 776-782.	6.7	52
140	Highâ€speed atmospheric atomic layer deposition of ultra thin amorphous TiO <sub>2</sub> blocking layers at 100 °C for inverted bulk heterojunction solar cells. Progress in Photovoltaics: Research and Applications, 2013, 21, 393-400.	8.1	52
141	Vertically aligned nanocomposite electrolytes with superior out-of-plane ionic conductivity for solid oxide fuel cells. Journal of Power Sources, 2013, 242, 455-463.	7.8	52
142	Size-dependent radiation tolerance in ion irradiated TiN/AlN nanolayer films. Journal of Nuclear Materials, 2013, 441, 47-53.	2.7	52
143	Sharp semiconductor-to-metal transition of VO2 thin films on glass substrates. Journal of Applied Physics, 2013, 114, .	2.5	52
144	Composite epitaxial thin films: A new platform for tuning, probing, and exploiting mesoscale oxides. MRS Bulletin, 2015, 40, 933-942.	3.5	52

#	Article	IF	CITATIONS
145	Epitaxial Growth of 1D Atomic Chain Based Se Nanoplates on Monolayer ReS <sub>2</sub> for Highâ€Performance Photodetectors. Advanced Functional Materials, 2018, 28, 1806254.	14.9	52
146	Perovskite Transparent Conducting Oxide for the Design of a Transparent, Flexible, and Self-Powered Perovskite Photodetector. ACS Applied Materials & Interfaces, 2020, 12, 16462-16468.	8.0	52
147	Design of Radiation Tolerant Nanostructured Metallic Multilayers. Journal of Engineering Materials and Technology, Transactions of the ASME, 2012, 134, .	1.4	51
148	Thermal stability of twins and strengthening mechanisms in differently oriented epitaxial nanotwinned Ag films. Journal of Materials Research, 2013, 28, 1729-1739.	2.6	51
149	Very High Surface Area Mesoporous Thin Films of SrTiO <sub>3</sub> Grown by Pulsed Laser Deposition and Application to Efficient Photoelectrochemical Water Splitting. Nano Letters, 2016, 16, 7338-7345.	9.1	51
150	Preparation of bulk ultrafine-grained and nanostructured Zn, Al and their alloys by in situ consolidation of powders during mechanical attrition. Scripta Materialia, 2002, 46, 661-665.	5.2	50
151	Nanostructured cathode thin films with vertically-aligned nanopores for thin film SOFC and their characteristics. Applied Surface Science, 2007, 254, 266-269.	6.1	50
152	Structural and dielectric properties of epitaxial Sm2O3 thin films. Applied Physics Letters, 2008, 92, 062905.	3.3	50
153	Couplings of Polarization with Interfacial Deep Trap and Schottky Interface Controlled Ferroelectric Memristive Switching. Advanced Functional Materials, 2020, 30, 2000664.	14.9	50
154	Precise Tuning of (YBa <sub>2</sub> Cu <sub>3</sub> O <sub>7â€Ĩ</sub> ) <sub>1â€x</sub> :(BaZrO <sub>3</sub> ) <sub>x</sub> Thin Film Nanocomposite Structures. Advanced Functional Materials, 2014, 24, 5240-5245.	14.9	49
155	Epitaxial growth of ZnO films on Si(111). Journal of Materials Research, 2002, 17, 2480-2483.	2.6	48
156	Epitaxial Superconducting Î'-MoN Films Grown by a Chemical Solution Method. Journal of the American Chemical Society, 2011, 133, 20735-20737.	13.7	48
157	The formation mechanisms of growth twins in polycrystalline Al with high stacking fault energy. Acta Materialia, 2015, 101, 62-70.	7.9	48
158	Microstructure and mechanical behavior of nanotwinned AlTi alloys with 9R phase. Scripta Materialia, 2018, 148, 5-9.	5.2	48
159	Ferroelectric Properties of Vertically Aligned Nanostructured BaTiO <sub>3</sub> –CeO <sub>2</sub> Thin Films and Their Integration on Silicon. ACS Applied Materials & Interfaces, 2013, 5, 12541-12547.	8.0	47
160	Superior tolerance of Ag/Ni multilayers against Kr ion irradiation: an <i>in situ</i> study. Philosophical Magazine, 2013, 93, 3547-3562.	1.6	47
161	Plasticity and ultra-low stress induced twin boundary migration in nanotwinned Cu by <i>in situ</i> nanoindentation studies. Applied Physics Letters, 2014, 104, .	3.3	47
162	Comparison of the grain growth behavior and defect structures of flash sintered ZnO with and without controlled current ramp. Scripta Materialia, 2019, 162, 251-255.	5.2	47

#	Article	IF	CITATIONS
163	Strong room temperature exchange bias in self-assembled BiFeO3–Fe3O4 nanocomposite heteroepitaxial films. Applied Physics Letters, 2013, 102, .	3.3	46
164	Resonance Raman spectroscopy of G-line and folded phonons in twisted bilayer graphene with large rotation angles. Applied Physics Letters, 2013, 103, .	3.3	46
165	Laser-Induced Mesoporous Nickel Oxide as a Highly Sensitive Nonenzymatic Glucose Sensor. ACS Applied Nano Materials, 2020, 3, 5260-5270.	5.0	46
166	Hysteretic Vortex Pinning in Superconductor-Ferromagnet Nanocomposites. Physical Review Letters, 2007, 98, 117003.	7.8	45
167	Protective nitride formation on stainless steel alloys for proton exchange membrane fuel cell bipolar plates. Journal of Power Sources, 2007, 174, 228-236.	7.8	45
168	Fluence-dependent radiation damage in helium (He) ion-irradiated Cu/V multilayers. Philosophical Magazine, 2013, 93, 883-898.	1.6	45
169	Strain relaxation and enhanced perpendicular magnetic anisotropy in BiFeO3:CoFe2O4 vertically aligned nanocomposite thin films. Applied Physics Letters, 2014, 104, .	3.3	45
170	High temperature thermal and mechanical stability of high-strength nanotwinned Al alloys. Acta Materialia, 2019, 165, 142-152.	7.9	45
171	Chemical Solution Deposition of Epitaxial Carbide Films. Journal of the American Chemical Society, 2010, 132, 2516-2517.	13.7	44
172	Microstructural and magnetic properties of (La0.7Sr0.3MnO3)0.7:(Mn3O4)0.3 nanocomposite thin films. Journal of Applied Physics, 2011, 109, .	2.5	44
173	Single-Crystalline Thin Films for Studying Intrinsic Properties of BiFeO <sub>3</sub> –SrTiO <sub>3</sub> Solid Solution Photoelectrodes in Solar Energy Conversion. Chemistry of Materials, 2015, 27, 6635-6641.	6.7	44
174	The effects of external fields in ceramic sintering. Journal of the American Ceramic Society, 2019, 102, 5-31.	3.8	44
175	Formation of epitaxial Au/Ni/Au ohmic contacts to p-GaN. Applied Physics Letters, 2002, 81, 3978-3980.	3.3	43
176	Controlling factors in tensile deformation of nanocrystalline cobalt and nickel. Physical Review B, 2012, 85, .	3.2	43
177	Transparent p-type epitaxial thin films of nickel oxide. Chemical Communications, 2014, 50, 1854.	4.1	43
178	Vertical-Interface-Manipulated Conduction Behavior in Nanocomposite Oxide Thin Films. ACS Applied Materials & Interfaces, 2014, 6, 5356-5361.	8.0	43
179	Strong perpendicular exchange bias in epitaxial La <sub>0.7</sub> Sr <sub>0.3</sub> MnO <sub>3</sub> :BiFeO <sub>3</sub> nanocomposite films through vertical interfacial coupling. Nanoscale, 2015, 7, 13808-13815.	5.6	43
180	Real-time in situ optical tracking of oxygen vacancy migration in memristors. Nature Electronics, 2020, 3, 687-693.	26.0	43

#	Article	IF	CITATIONS
181	Rapid Upcycling of Waste Polyethylene Terephthalate to Energy Storing Disodium Terephthalate Flowers with DFT Calculations. ACS Sustainable Chemistry and Engineering, 2020, 8, 6252-6262.	6.7	43
182	Investigation of strengthening mechanisms in an additively manufactured Haynes 230 alloy. Acta Materialia, 2022, 222, 117404.	7.9	43
183	Orientation-dependent hardness and strain rate sensitivity in nanotwin copper. Applied Physics Letters, 2012, 100, .	3.3	42
184	Oxygen-Vacancy-Induced Antiferromagnetism to Ferromagnetism Transformation in Eu0.5Ba0.5TiO3â~δ Multiferroic Thin Films. Scientific Reports, 2013, 3, 2618.	3.3	42
185	Growth of thick Yba <sub>2</sub> Cu <sub>3</sub> O <sub>7â^î</sub> films carrying a critical current of over 230 A/cm on single LaMnO <sub>3</sub> -buffered ion-beam assisted deposition MgO substrates. Journal of Materials Research, 2003, 18, 2055-2059.	2.6	41
186	Pre-oxidized and nitrided stainless steel alloy foil for proton exchange membrane fuel cell bipolar plates: Part 1. Corrosion, interfacial contact resistance, and surface structure. Journal of Power Sources, 2010, 195, 5610-5618.	7.8	41
187	Textured metastable VO2 (B) thin films on SrTiO3 substrates with significantly enhanced conductivity. Applied Physics Letters, 2014, 104, .	3.3	41
188	In situ study of heavy ion irradiation response of immiscible Cu/Fe multilayers. Journal of Nuclear Materials, 2016, 475, 274-279.	2.7	41
189	Copper diffusion characteristics in single-crystal and polycrystalline TaN. Applied Physics Letters, 2002, 81, 1453-1455.	3.3	40
190	Microstructure of SrTiO3 buffer layers and itseffects on superconducting properties ofYBa2Cu3O7-δ coated conductors. Journal of Materials Research, 2004, 19, 1869-1875.	2.6	40
191	Growth-controlled surface roughness in Al-doped ZnO as transparent conducting oxide. Nanotechnology, 2009, 20, 395704.	2.6	40
192	Amorphization of nanocrystalline 3C-SiC irradiated with Si <sup>+</sup> ions. Journal of Materials Research, 2010, 25, 2341-2348.	2.6	40
193	Perpendicular Exchange-Biased Magnetotransport at the Vertical Heterointerfaces in La <sub>0.7</sub> Sr <sub>0.3</sub> MnO <sub>3</sub> :NiO Nanocomposites. ACS Applied Materials & Interfaces, 2015, 7, 21646-21651.	8.0	40
194	Bioinspired Dynamic Camouflage from Colloidal Nanocrystals Embedded Electrochromics. Nano Letters, 2021, 21, 4500-4507.	9.1	40
195	Role of silver addition in the synthesis of high critical current density MgB2bulk superconductors. Superconductor Science and Technology, 2003, 16, 455-458.	3.5	39
196	Strong room temperature magnetism in highly resistive strained thin films of BiFe0.5Mn0.5O3. Applied Physics Letters, 2011, 98, .	3.3	39
197	A new method for reliable determination of strain-rate sensitivity of low-dimensional metallic materials by using nanoindentation. Scripta Materialia, 2014, 77, 5-8.	5.2	39
198	Self-Assembled Magnetic Metallic Nanopillars in Ceramic Matrix with Anisotropic Magnetic and Electrical Transport Properties. ACS Applied Materials & Interfaces, 2016, 8, 20283-20291.	8.0	39

#	Article	IF	CITATIONS
199	Thermal stability of sputter-deposited 330 austenitic stainless-steel thin films with nanoscale growth twins. Applied Physics Letters, 2005, 87, 233116.	3.3	38
200	Room Temperature Ferrimagnetism and Ferroelectricity in Strained, Thin Films of BiFe <sub>0.5</sub> Mn <sub>0.5</sub> O <sub>3</sub> . Advanced Functional Materials, 2014, 24, 7478-7487.	14.9	38
201	Helium irradiation induced ultra-high strength nanotwinned Cu with nanovoids. Acta Materialia, 2019, 177, 107-120.	7.9	38
202	Ge2Sb2Se5 Glass as High-capacity Promising Lithium-ion Battery Anode. Nano Energy, 2020, 68, 104326.	16.0	38
203	Metal-Free Oxide-Nitride Heterostructure as a Tunable Hyperbolic Metamaterial Platform. Nano Letters, 2020, 20, 6614-6622.	9.1	38
204	The influence of stacking faults on mechanical behavior of advanced materials. Materials Science & Engineering A: Structural Materials: Properties, Microstructure and Processing, 2021, 803, 140696.	5.6	38
205	Advances in synthesis and applications of boron nitride nanotubes: A review. Chemical Engineering Journal, 2022, 431, 134118.	12.7	38
206	The role of a superconducting seed layer in the structural and transport properties of EuBa2Cu3O7â^'x films. Applied Physics Letters, 2003, 83, 1388-1390.	3.3	37
207	Strengthening mechanisms in nanostructured copper/304 stainless steel multilayers. Journal of Materials Research, 2003, 18, 1600-1606.	2.6	37
208	Controlling Crystal Structure and Oxidation State in Molybdenum Nitrides through Epitaxial Stabilization. Journal of Physical Chemistry C, 2011, 115, 17880-17883.	3.1	37
209	New strain states and radical property tuning of metal oxides using a nanocomposite thin film approach. APL Materials, 2015, 3, 062507.	5.1	37
210	Hybrid plasmonic Au–TiN vertically aligned nanocomposites: a nanoscale platform towards tunable optical sensing. Nanoscale Advances, 2019, 1, 1045-1054.	4.6	37
211	A high-entropy manganite in an ordered nanocomposite for long-term application in solid oxide cells. Nature Communications, 2021, 12, 2660.	12.8	37
212	In situ heavy ion irradiation studies of nanopore shrinkage and enhanced radiation tolerance of nanoporous Au. Scientific Reports, 2017, 7, 39484.	3.3	37
213	Mechanical properties of nanocrystalline and epitaxial TiN films on (100) silicon. Journal of Materials Research, 2001, 16, 2733-2738.	2.6	36
214	Modulated oscillatory hardening and dynamic recrystallization in cryomilled nanocrystalline Zn. Acta Materialia, 2002, 50, 3995-4004.	7.9	36
215	Microstructure and transport properties of Y-rich YBa2Cu3O7â^î^ thin films. Journal of Applied Physics, 2006, 100, 053904.	2.5	36
216	Tunable lattice strain in vertically aligned nanocomposite (BiFeO3)x:(Sm2O3)1â^'x thin films. Journal of Applied Physics, 2009, 106, .	2.5	36

#	Article	IF	CITATIONS
217	Enhanced low-field magnetoresistance in La0.67Sr0.33MnO3:MgO composite films. Journal of Applied Physics, 2011, 110, .	2.5	36
218	A formation mechanism for ultra-thin nanotwins in highly textured Cu/Ni multilayers. Journal of Applied Physics, 2012, 111, .	2.5	36
219	Hydrogen sorption in orthorhombic Mg hydride at ultra-low temperature. International Journal of Hydrogen Energy, 2013, 38, 8328-8341.	7.1	36
220	Selfâ€Organized Epitaxial Vertically Aligned Nanocomposites with Longâ€Range Ordering Enabled by Substrate Nanotemplating. Advanced Materials, 2017, 29, 1606861.	21.0	36
221	Texture-directed twin formation propensity in Al with high stacking fault energy. Acta Materialia, 2018, 144, 226-234.	7.9	36
222	Exchange Bias in a La <sub>0.67</sub> Sr <sub>0.33</sub> MnO <sub>3</sub> /NiO Heterointerface Integrated on a Flexible Mica Substrate. ACS Applied Materials & Interfaces, 2020, 12, 39920-39925.	8.0	36
223	Epitaxial growth of TaN thin films on Si(100) and Si(111) using a TiN buffer layer. Applied Physics Letters, 2002, 80, 2323-2325.	3.3	35
224	Epitaxial growth of Eu2O3 thin films on LaAlO3 substrates by polymer-assisted deposition. Applied Physics Letters, 2004, 85, 3426-3428.	3.3	35
225	Enhanced flux pinning in YBa2Cu3O7â <sup>~</sup> δthin films using Nb-based double perovskite additions. Superconductor Science and Technology, 2010, 23, 022003.	3.5	35
226	Enhanced critical current in YBa <sub>2</sub> Cu <sub>3</sub> O <sub>7â<sup>~</sup>δ</sub> thin films through pinning by ferromagnetic YFeO <sub>3</sub> nanoparticles. Superconductor Science and Technology, 2010, 23, 045019.	3.5	35
227	TiN-based coatings on fuel cladding tubes for advanced nuclear reactors. Journal of Nuclear Materials, 2012, 429, 143-148.	2.7	35
228	Optical limiting properties in copper oxide thin films under a high-repetition-rate femtosecond laser. Materials Letters, 2013, 91, 319-322.	2.6	35
229	Solar-Blind UV Photodetector Based on Atomic Layer-Deposited Cu <sub>2</sub> O and Nanomembrane β-Ga <sub>2</sub> O <sub>3</sub> pn Oxide Heterojunction. ACS Omega, 2019, 4, 20756-20761.	3.5	35
230	Magnetotransport properties of quasi-one-dimensionally channeled vertically aligned heteroepitaxial nanomazes. Applied Physics Letters, 2013, 102, .	3.3	34
231	Strong pinning in very fast grown reactive co-evaporated GdBa2Cu3O7 coated conductors. APL Materials, 2014, 2, .	5.1	34
232	Enhanced radiation tolerance in immiscible Cu/Fe multilayers with coherent and incoherent layer interfaces. Journal of Materials Research, 2015, 30, 1300-1309.	2.6	34
233	Tailorable Au Nanoparticles Embedded in Epitaxial TiO <sub>2</sub> Thin Films for Tunable Optical Properties. ACS Applied Materials & Interfaces, 2018, 10, 32895-32902.	8.0	34
234	Self-assembled vertically aligned Ni nanopillars in CeO <sub>2</sub> with anisotropic magnetic and transport properties for energy applications. Nanoscale, 2018, 10, 17182-17188.	5.6	34

#	Article	IF	CITATIONS
235	Thick grain boundary induced strengthening in nanocrystalline Ni alloy. Nanoscale, 2019, 11, 23449-23458.	5.6	34
236	Evolution of microstructure and mechanical properties of in situ consolidated bulk ultra-fine-grained and nanocrystalline Zn prepared by ball milling. Materials Science & Engineering A: Structural Materials: Properties, Microstructure and Processing, 2003, 344, 175-181.	5.6	33
237	Flux pinning in YBa2Cu3O7â^1̂´ thin film samples linked to stacking fault density. Applied Physics Letters, 2008, 92, 082507.	3.3	33
238	Strengthening mechanisms of Ag/Ni immiscible multilayers with fcc/fcc interface. Surface and Coatings Technology, 2013, 237, 269-275.	4.8	33
239	Electric-Field Control of Ferromagnetism in a Nanocomposite via a ZnO Phase. Nano Letters, 2013, 13, 5886-5890.	9.1	33
240	Evolution of microstructure, strain and physical properties in oxide nanocomposite films. Scientific Reports, 2014, 4, 5426.	3.3	33
241	Exchange Bias Effect along Vertical Interfaces in La0.7Sr0.3MnO3:NiO Vertically Aligned Nanocomposite Thin Films Integrated on Silicon Substrates. Crystal Growth and Design, 2018, 18, 4388-4394.	3.0	33
242	He ion irradiation response of a gradient T91 steel. Acta Materialia, 2020, 196, 175-190.	7.9	33
243	Effect of microstructure on diffusion of copper in TiN films. Journal of Applied Physics, 2003, 93, 5210-5214.	2.5	32
244	A Chemical Solution Approach to Epitaxial Metal Nitride Thin Films. Advanced Materials, 2009, 21, 193-197.	21.0	32
245	An experimental and modeling study on the role of damage cascade formation in nanocrystalization of ion-irradiated Ni52.5Nb10Zr15Ti15Pt7.5 metallic glass. Scripta Materialia, 2010, 63, 1045-1048.	5.2	32
246	Electrochemical characterization of YBaCo3ZnO7+Gd0.2Ce0.8O1.9 composite cathodes for intermediate temperature solid oxide fuel cells. Electrochimica Acta, 2010, 55, 5312-5317.	5.2	32
247	Thermal stability of ultrafine grained Fe–Cr–Ni alloy. Materials Science & Engineering A: Structural Materials: Properties, Microstructure and Processing, 2012, 542, 64-70.	5.6	32
248	Diffusion barrier properties of nitride-based coatings on fuel cladding. Journal of Alloys and Compounds, 2013, 580, 442-448.	5.5	32
249	Size and stress dependent hydrogen desorption in metastable Mg hydride films. International Journal of Hydrogen Energy, 2014, 39, 2597-2607.	7.1	32
250	Tailorable Optical Response of Au–LiNbO <sub>3</sub> Hybrid Metamaterial Thin Films for Optical Waveguide Applications. Advanced Optical Materials, 2018, 6, 1800510.	7.3	32
251	High strength, deformable nanotwinned Al–Co alloys. Materials Research Letters, 2019, 7, 33-39.	8.7	32
252	Tailoring strength and plasticity of Ag/Nb nanolaminates via intrinsic microstructure and extrinsic dimension. International Journal of Plasticity, 2019, 113, 145-157.	8.8	32

#	Article	IF	CITATIONS
253	Manipulating Magnetoresistance Near Room Temperature in La0.67Sr0.33MnO3/La0.67Ca0.33MnO3 Films Prepared by Polymer Assisted Deposition. Advanced Materials, 2006, 18, 2695-2698.	21.0	31
254	Self-assembled multilayers and enhanced superconductivity in (YBa2Cu3O7â^'x)0.5:(BaZrO3)0.5 nanocomposite films. Journal of Applied Physics, 2009, 106, .	2.5	31
255	Electrochemical and Structural Effects of In Situ Li <sub>2</sub> O Extraction from Li <sub>2</sub> MnO <sub>3</sub> for Li-Ion Batteries. ACS Applied Materials & Interfaces, 2015, 7, 2433-2438.	8.0	31
256	Study of the Flux Pinning Landscape of YBCO Thin Films With Single and Mixed Phase Additions BaMO3 + Z: M = Hf, Sn, Zr and Z = Y2O3, Y211. IEEE Transactions on Applied Superconductivity, 2017, 27, 1-5.	1.7	31
257	In situ measurement of temperature and reduction of rutile titania using energy dispersive x-ray diffraction. Journal of the European Ceramic Society, 2018, 38, 5503-5511.	5.7	31
258	3D strain-induced superconductivity in La <sub>2</sub> CuO <sub>4+î´</sub> using a simple vertically aligned nanocomposite approach. Science Advances, 2019, 5, eaav5532.	10.3	31
259	Selfâ€Assembled Ag–TiN Hybrid Plasmonic Metamaterial: Tailorable Tilted Nanopillar and Optical Properties. Advanced Optical Materials, 2019, 7, 1801180.	7.3	31
260	Strong and plastic metallic composites with nanolayered architectures. Acta Materialia, 2020, 195, 240-251.	7.9	31
261	Role of ALD Al <sub>2</sub> O <sub>3</sub> Surface Passivation on the Performance of p-Type Cu <sub>2</sub> O Thin Film Transistors. ACS Applied Materials & Interfaces, 2021, 13, 4156-4164.	8.0	31
262	Comparative Study of <tex>\$rm REBa_2rm Cu_3rm O_7\$</tex> Films for Coated Conductors. IEEE Transactions on Applied Superconductivity, 2005, 15, 2723-2726.	1.7	30
263	A New Material for Highâ€Temperature Leadâ€Free Actuators. Advanced Functional Materials, 2013, 23, 5881-5886.	14.9	30
264	Strain-induced suppression of the miscibility gap in nanostructured Mg <sub>2</sub> Si–Mg <sub>2</sub> Sn solid solutions. Journal of Materials Chemistry A, 2018, 6, 17559-17570.	10.3	30
265	Plasmonic Cu nanostructures in ZnO as hyperbolic metamaterial thin films. Materials Today Nano, 2019, 8, 100052.	4.6	30
266	Strain-driven nanodumbbell structure and enhanced physical properties in hybrid vertically aligned nanocomposite thin films. Applied Materials Today, 2019, 16, 204-212.	4.3	30
267	Strain-Driven In-plane Ordering in Vertically Aligned ZnO–Au Nanocomposites with Highly Correlated Metamaterial Properties. ACS Omega, 2020, 5, 2234-2241.	3.5	30
268	Characterization of precipitation in gradient Inconel 718 superalloy. Materials Science & Engineering A: Structural Materials: Properties, Microstructure and Processing, 2021, 804, 140718.	5.6	30
269	Cs-Corrected Scanning Transmission Electron Microscopy Investigation of Dislocation Core Configurations at a SrTiO3/MgO Heterogeneous Interface. Microscopy and Microanalysis, 2013, 19, 706-715.	0.4	29
270	Vertically aligned nanocomposite La0.8Sr0.2MnO3â^î/̈/Zr0.92Y0.08O1.96 thin films as electrode/electrolyte interfacial layer for solid oxide reversible fuel cells. International Journal of Hydrogen Energy, 2013, 38, 16320-16327.	7.1	29

#	Article	IF	CITATIONS
271	Research Updates: Epitaxial strain relaxation and associated interfacial reconstructions: The driving force for creating new structures with integrated functionality. APL Materials, 2013, 1, .	5.1	29
272	Vertically Aligned Nanocomposite BaTiO <sub>3</sub> :YMnO <sub>3</sub> Thin Films with Room Temperature Multiferroic Properties toward Nanoscale Memory Devices. ACS Applied Nano Materials, 2018, 1, 2509-2514.	5.0	29
273	Effect of thickness variation in high-efficiency InGaN/GaN light-emitting diodes. Applied Physics Letters, 2002, 81, 841-843.	3.3	28
274	Critical current density and microstructure variations in YBa <sub>2</sub> Cu <sub>3</sub> O <sub>7â^</sub> <i><sub>x</sub></i> + BaSnO <sub>3</sub> films with different concentrations of BaSnO <sub>3</sub> . Journal of Materials Research, 2008, 23, 3363-3369.	2.6	28
275	The role of interfacial defects in enhancing the critical current density of YBa <sub>2</sub> Cu <sub>3</sub> O <sub>7â^Î</sub> coatings. Superconductor Science and Technology, 2009, 22, 125002.	3.5	28
276	Grain and grain boundary activities observed in alumina–zirconia–magnesia spinel nanocomposites by in situ nanoindentation using transmission electron microscopy. Acta Materialia, 2010, 58, 4891-4899.	7.9	28
277	Two Types of Martensitic Phase Transformations in Magnetic Shape Memory Alloys by Inâ€ <b>S</b> itu Nanoindentation Studies. Advanced Materials, 2014, 26, 3893-3898.	21.0	28
278	Self-Assembled Heteroepitaxial Oxide Nanocomposite for Photoelectrochemical Solar Water Oxidation. Chemistry of Materials, 2016, 28, 3017-3023.	6.7	28
279	Synthesis of bulk nanostructured Zn by combinations of cryomilling and powder consolidation by room temperature milling: optimizing mechanical properties. Scripta Materialia, 2003, 49, 429-433.	5.2	27
280	Vortex pinning landscape in YBa <sub>2</sub> Cu <sub>3</sub> O <sub>7</sub> films grown by hybrid liquid phase epitaxy. Superconductor Science and Technology, 2007, 20, S223-S229.	3.5	27
281	Practical Magnetic Pinning in YBCO. IEEE Transactions on Applied Superconductivity, 2009, 19, 3148-3151.	1.7	27
282	Much simplified ion-beam assisted deposition-TiN template for high-performance coated conductors. Journal of Applied Physics, 2010, 108, .	2.5	27
283	Heterointerface design and strain tuning in epitaxial BiFeO3:CoFe2O4 nanocomposite films. Applied Physics Letters, 2015, 107, .	3.3	27
284	Superior twin stability and radiation resistance of nanotwinned Ag solid solution alloy. Acta Materialia, 2018, 151, 395-405.	7.9	27
285	Microscopic adaptation of BaHfO <sub>3</sub> and Y <sub>2</sub> O <sub>3</sub> artificial pinning centers for strong and isotropic pinning landscape in YBa <sub>2</sub> Cu <sub>3</sub> O <sub>7–<i>x</i></sub> thin films. Superconductor Science and Technology. 2018. 31. 025008.	3.5	27
286	In situ studies on irradiation resistance of nanoporous Au through temperature-jump tests. Acta Materialia, 2018, 143, 30-42.	7.9	27
287	Deformation mechanisms in FCC Co dominated by high-density stacking faults. Materials Science & Engineering A: Structural Materials: Properties, Microstructure and Processing, 2018, 736, 12-21.	5.6	27
288	9R phase enabled superior radiation stability of nanotwinned Cu alloys via in situ radiation at elevated temperature. Acta Materialia, 2019, 167, 248-256.	7.9	27

#	Article	IF	CITATIONS
289	Tunable Optical Properties in Selfâ€Assembled Oxideâ€Metal Hybrid Thin Films via Auâ€Phase Geometry Control: From Nanopillars to Nanodisks. Advanced Optical Materials, 2020, 8, 1901359.	7.3	27
290	Highly Conductive Copper–Silver Bimodal Paste for Low-Cost Printed Electronics. ACS Applied Electronic Materials, 2021, 3, 3352-3364.	4.3	27
291	Epitaxial Ternary Nitride Thin Films Prepared by a Chemical Solution Method. Journal of the American Chemical Society, 2008, 130, 15224-15225.	13.7	26
292	Highly Conductive Films of Layered Ternary Transitionâ€Metal Nitrides. Angewandte Chemie - International Edition, 2009, 48, 1490-1493.	13.8	26
293	Coexistence of strong ferromagnetism and polar switching at room temperature in Fe3O4–BiFeO3 nanocomposite thin films. Applied Physics Letters, 2010, 97, 153121.	3.3	26
294	Tilted Aligned Epitaxial La <sub>0.7</sub> Sr <sub>0.3</sub> MnO <sub>3</sub> Nanocolumnar Films with Enhanced Low-Field Magnetoresistance by Pulsed Laser Oblique-Angle Deposition. Crystal Growth and Design, 2011, 11, 5405-5409.	3.0	26
295	Basic criteria for formation of growth twins in high stacking fault energy metals. Applied Physics Letters, 2013, 103, .	3.3	26
296	In situ studies of radiation induced crystallization in Fe/a-Y2O3 nanolayers. Journal of Nuclear Materials, 2014, 452, 321-327.	2.7	26
297	Enhanced tunable magnetoresistance properties over a wide temperature range in epitaxial (La0.7Sr0.3MnO3)1â <sup>~7</sup> x:(CeO2)x nanocomposites. Journal of Applied Physics, 2015, 118, .	2.5	26
298	Aqueous Solution-Deposited Molybdenum Oxide Films as an Anode Interfacial Layer for Organic Solar Cells. ACS Applied Materials & Interfaces, 2015, 7, 18218-18224.	8.0	26
299	Two-Dimensional Layered Oxide Structures Tailored by Self-Assembled Layer Stacking via Interfacial Strain. ACS Applied Materials & Interfaces, 2016, 8, 16845-16851.	8.0	26
300	Broad Range Tuning of Phase Transition Property in VO <sub>2</sub> Through Metal eramic Nanocomposite Design. Advanced Functional Materials, 2019, 29, 1903690.	14.9	26
301	Response of solidification cellular structures in additively manufactured 316 stainless steel to heavy ion irradiation: an <i>in situ</i> study. Materials Research Letters, 2019, 7, 290-297.	8.7	26
302	Multifunctional Metal–Oxide Nanocomposite Thin Film with Plasmonic Au Nanopillars Embedded in Magnetic La <sub>0.67</sub> Sr <sub>0.33</sub> MnO <sub>3</sub> Matrix. Nano Letters, 2021, 21, 1032-1039.	9.1	26
303	Thermal stability of immiscible Cu-Ag/Fe triphase multilayers with triple junctions. Acta Materialia, 2021, 208, 116679.	7.9	26
304	Identification of the misfit dislocations at YBa2Cu3O7â~ʾĨ/SrTiO3 interface using moiré fringe contrast. Physica C: Superconductivity and Its Applications, 2006, 444, 1-4.	1.2	25
305	Transition from Irradiationâ€Induced Amorphization to Crystallization in Nanocrystalline Silicon Carbide. Journal of the American Ceramic Society, 2011, 94, 4127-4130.	3.8	25
306	Highly textured Li(Ni0.5Mn0.3Co0.2)O2 thin films on stainless steel as cathode forÂlithium-ion battery. Journal of Power Sources, 2013, 241, 410-414.	7.8	25

#	Article	IF	CITATIONS
307	Magnetic properties of (CoFe2O4)x:(CeO2)1â^'x vertically aligned nanocomposites and their pinning properties in YBa2Cu3O7â^'δ thin films. Journal of Applied Physics, 2014, 115, 123902.	2.5	25
308	A simplified superconducting coated conductor design with Fe-based superconductors on glass and flexible metallic substrates. Journal of Alloys and Compounds, 2015, 647, 380-385.	5.5	25
309	Turning antiferromagnetic Sm <sub>0.34</sub> Sr <sub>0.66</sub> MnO <sub>3</sub> into a 140 K ferromagnet using a nanocomposite strain tuning approach. Nanoscale, 2016, 8, 8083-8090.	5.6	25
310	Layer thickness dependent strain rate sensitivity of Cu/amorphous CuNb multilayer. Applied Physics Letters, 2017, 110, .	3.3	25
311	Novel Layered Supercell Structure from Bi <sub>2</sub> AlMnO <sub>6</sub> for Multifunctionalities. Nano Letters, 2017, 17, 6575-6582.	9.1	25
312	Study of deformation mechanisms in flash-sintered yttria-stabilized zirconia by <i>in-situ</i> micromechanical testing at elevated temperatures. Materials Research Letters, 2019, 7, 194-202.	8.7	25
313	Deformation behavior and phase transformation of nanotwinned Al/Ti multilayers. Applied Surface Science, 2020, 527, 146776.	6.1	25
314	Nitrideâ€Oxideâ€Metal Heterostructure with Selfâ€Assembled Core–Shell Nanopillar Arrays: Effect of Ordering on Magnetoâ€Optical Properties. Small, 2021, 17, e2007222.	10.0	25
315	Thickness effects of SrTiO3 buffer layers on superconducting properties of YBa2Cu3O7â^î^ coated conductors. Physica C: Superconductivity and Its Applications, 2005, 433, 43-49.	1.2	24
316	Size dependent strengthening mechanisms in sputtered Fe/W multilayers. Journal of Applied Physics, 2010, 107, 093503.	2.5	24
317	A chemical solution approach for superconducting and hard epitaxial NbC film. Chemical Communications, 2010, 46, 7837.	4.1	24
318	A new approach to investigate Li <sub>2</sub> MnO <sub>3</sub> and Li(Ni <sub>0.5</sub> Mn <sub>0.3</sub> Co <sub>0.2</sub> )O <sub>2</sub> mixed phase cathode materials. Journal of Materials Chemistry A, 2014, 2, 2283-2289.	10.3	24
319	Roles of strain and domain boundaries on the phase transition stability of VO2 thin films. Applied Physics Letters, 2017, 111, .	3.3	24
320	Radiation induced detwinning in nanotwinned Cu. Scripta Materialia, 2017, 130, 37-41.	5.2	24
321	Microstructure, Magnetic, and Magnetoresistance Properties of La0.7Sr0.3MnO3:CuO Nanocomposite Thin Films. ACS Applied Materials & Interfaces, 2018, 10, 5779-5784.	8.0	24
322	Design of a Vertical Composite Thin Film System with Ultralow Leakage To Yield Large Converse Magnetoelectric Effect. ACS Applied Materials & Interfaces, 2018, 10, 18237-18245.	8.0	24
323	Key microstructural characteristics in flash sintered 3YSZ critical for enhanced sintering process. Ceramics International, 2019, 45, 1251-1257.	4.8	24
324	Interface Engineered Roomâ€Temperature Ferromagnetic Insulating State in Ultrathin Manganite Films. Advanced Science, 2020, 7, 1901606.	11.2	24

#	Article	IF	CITATIONS
325	Ultra-high strength and plasticity mediated by partial dislocations and defect networks: Part I: Texture effect. Acta Materialia, 2020, 185, 181-192.	7.9	24
326	Flash sintering incubation kinetics. Npj Computational Materials, 2020, 6, .	8.7	24
327	Thermal stability and deformability of annealed nanotwinned Al/Ti multilayers. Scripta Materialia, 2020, 186, 219-224.	5.2	24
328	Defects in flash-sintered ceramics and their effects on mechanical properties. MRS Bulletin, 2021, 46, 44-51.	3.5	24
329	Crossover of thickness dependence of critical current density Jc(T,H) in YBa2Cu3O7â^'δ thick films. Applied Physics Letters, 2004, 84, 3528-3530.	3.3	23
330	Mechanical behavior of nanostructured materials symposium honoring Carl Koch. Jom, 2007, 59, 49-49.	1.9	23
331	Elevated temperature deformation behavior of spark plasma sintered nanometric nickel with varied grain size distributions. Materials Science & Engineering A: Structural Materials: Properties, Microstructure and Processing, 2010, 528, 663-671.	5.6	23
332	Magnetic Properties of Self-Assembled Epitaxial Nanocomposite CoFe2O4:SrTiO3 and CoFe2O4:MgO Films. Journal of Physical Chemistry C, 2011, 115, 25338-25342.	3.1	23
333	Monolithic Mid-Infrared Integrated Photonics Using Silicon-on-Epitaxial Barium Titanate Thin Films. ACS Applied Materials & Interfaces, 2017, 9, 21848-21855.	8.0	23
334	Phase transformation induced plasticity in high-strength hexagonal close packed Co with stacking faults. Scripta Materialia, 2019, 173, 32-36.	5.2	23
335	Review on the growth, properties and applications of self-assembled oxide–metal vertically aligned nanocomposite thin films—current and future perspectives. Materials Horizons, 2021, 8, 869-884.	12.2	23
336	Wireless Humidity Sensor for Smart Packaging via Oneâ€step Laserâ€Induced Patterning and Nanoparticle Formation on Metallized Paper. Advanced Electronic Materials, 2022, 8, .	5.1	23
337	Emergent multiferroism with magnetodielectric coupling in EuTiO3 created by a negative pressure control of strong spin-phonon coupling. Nature Communications, 2022, 13, 2364.	12.8	23
338	High tunability of lead strontium titanate thin films using a conductive LaNiO3 as electrodes. Applied Physics Letters, 2007, 91, 072908.	3.3	22
339	Role of boundaries on low-field magnetotransport properties of La <sub>0.7</sub> Sr <sub>0.3</sub> MnO <sub>3</sub> -based nanocomposite thin films. Journal of Materials Research, 2013, 28, 1707-1714.	2.6	22
340	Strain and Interface Effects in a Novel Bismuth-Based Self-Assembled Supercell Structure. ACS Applied Materials & Interfaces, 2015, 7, 11631-11636.	8.0	22
341	Resilient ZnO nanowires in an irradiation environment: An in situ study. Acta Materialia, 2015, 95, 156-163.	7.9	22
342	Strong perpendicular exchange bias in epitaxial La0.7Sr0.3MnO3:LaFeO3 nanocomposite thin films. APL Materials, 2016, 4, .	5.1	22

#	Article	IF	CITATIONS
343	Influence of layer thickness on mechanical properties of multilayered NiFe samples processed by electrodeposition. Materials and Design, 2016, 90, 389-395.	7.0	22
344	Very high commutation quality factor and dielectric tunability in nanocomposite SrTiO <sub>3</sub> thin films with <i>T</i> <sub>c</sub> enhanced to >300 ŰC. Nanoscale, 2018, 10, 3460-3468.	5.6	22
345	Probing the effect of interface on vortex pinning efficiency of one-dimensional BaZrO3 and BaHfO3 artificial pinning centers in YBa2Cu3O7-x thin films. Applied Physics Letters, 2018, 113, .	3.3	22
346	Spontaneous Ordering of Oxide-Oxide Epitaxial Vertically Aligned Nanocomposite Thin Films. Annual Review of Materials Research, 2020, 50, 229-253.	9.3	22
347	Advanced Thin Film Cathodes for Lithium Ion Batteries. Research, 2020, 2020, 2969510.	5.7	22
348	The role of stacking faults in the critical current density of MOD films through a thickness dependence study. Superconductor Science and Technology, 2009, 22, 015022.	3.5	21
349	Enhanced ion irradiation tolerance properties in TiN/MgO nanolayer films. Journal of Nuclear Materials, 2013, 434, 217-222.	2.7	21
350	Radiation damage in heteroepitaxial BaTiO3 thin films on SrTiO3 under Ne ion irradiation. Journal of Applied Physics, 2013, 113, .	2.5	21
351	Vertical Interface Induced Dielectric Relaxation in Nanocomposite (BaTiO3)1-x:(Sm2O3)x Thin Films. Scientific Reports, 2015, 5, 11335.	3.3	21
352	Radiation tolerant nanocrystalline ZrN films under high dose heavy-ion irradiations. Journal of Applied Physics, 2015, 117, .	2.5	21
353	In Situ Studies on the Irradiation-Induced Twin Boundary-Defect Interactions in Cu. Metallurgical and Materials Transactions A: Physical Metallurgy and Materials Science, 2017, 48, 5172-5180.	2.2	21
354	Plastic anisotropy and tension-compression asymmetry in nanotwinned Al–Fe alloys: An in-situ micromechanical investigation. International Journal of Plasticity, 2020, 132, 102760.	8.8	21
355	Ultra-fine-grained and gradient FeCrAl alloys with outstanding work hardening capability. Acta Materialia, 2021, 215, 117049.	7.9	21
356	Mechanical properties of cyromilled nanocrystalline Zn studied by the miniaturized disk bend test. Acta Materialia, 2002, 50, 3527-3533.	7.9	20
357	Effect of crystallinity on the transport properties of Nd0.67Sr0.33MnO3 thin films. Applied Physics Letters, 2004, 84, 1147-1149.	3.3	20
358	Influence of deposition rate on the formation of growth twins in sputter-deposited 330 austenitic stainless steel films. Applied Physics Letters, 2007, 90, 153101.	3.3	20
359	Mixed-Valence Perovskite Thin Films by Polymer-Assisted Deposition. Journal of the American Ceramic Society, 2008, 91, 1858-1863.	3.8	20
360	Improved microstructure and enhanced low-field <i>J</i> <sub>c</sub> in (Y <sub>0.67</sub> Eu <sub>0.33</sub> )Ba <sub>2</sub> Cu <sub>3</sub> O <sub>7â^î(</sub> films. Superconductor Science and Technology, 2008, 21, 025001.	3.5	20

#	Article	IF	CITATIONS
361	Optimizing Flux Pinning of YBCO Superconductor With \$ hbox{BaSnO}_{3} + hbox{Y}_{2}hbox{O}_{3}\$ Dual Mixed Phase Additions. IEEE Transactions on Applied Superconductivity, 2013, 23, 8002104-8002104.	1.7	20
362	Temperature and grain size dependent plastic instability and strain rate sensitivity of ultrafine grained austenitic Fe–14Cr–16Ni alloy. Materials Science & Engineering A: Structural Materials: Properties, Microstructure and Processing, 2014, 597, 415-421.	5.6	20
363	Nanopillar Spin Filter Tunnel Junctions with Manganite Barriers. Nano Letters, 2014, 14, 2789-2793.	9.1	20
364	<i>In situ</i> Observation of Defect Annihilation in Kr Ion-Irradiated Bulk Fe/Amorphous-Fe <sub>2</sub> Zr Nanocomposite Alloy. Materials Research Letters, 2015, 3, 35-42.	8.7	20
365	Transformational dynamics of BZO and BHO nanorods imposed by Y2O3 nanoparticles for improved isotropic pinning in YBa2Cu3O7-δ thin films. AIP Advances, 2017, 7, .	1.3	20
366	Strain tuning of ferroelectric and optical properties of rhombohedral-like BiFeO3 thin films on SrRuO3-buffered substrates. Materials Research Bulletin, 2019, 110, 120-125.	5.2	20
367	Tailoring the thermal stability of nanocrystalline Ni alloy by thick grain boundaries. Scripta Materialia, 2020, 182, 21-26.	5.2	20
368	Vertically Aligned Ag <sub><i>x</i></sub> Au <sub>1–<i>x</i></sub> Alloyed Nanopillars Embedded in ZnO as Nanoengineered Low-Loss Hybrid Plasmonic Metamaterials. Nano Letters, 2020, 20, 3778-3785.	9.1	20
369	Carbon Nanotube Supported Amorphous MoS <sub>2</sub> via Microwave Heating Synthesis for Enhanced Performance of Hydrogen Evolution Reaction. Energy Material Advances, 2021, 2021, .	11.0	20
370	Guidelines for optimizing random and correlated pinning in rare-earth-based superconducting films. Superconductor Science and Technology, 2006, 19, S55-S59.	3.5	19
371	Conduction mechanisms of epitaxial EuTiO3 thin films. Applied Physics Letters, 2012, 101, .	3.3	19
372	Structure and magnetotransport properties of epitaxial nanocomposite La0.67Ca0.33MnO3:SrTiO3 thin films grown by a chemical solution approach. Applied Physics Letters, 2012, 100, 082403.	3.3	19
373	High quality p-type Ag-doped ZnO thin films achieved under elevated growth temperatures. Journal of Physics Condensed Matter, 2012, 24, 145802.	1.8	19
374	Effective magnetic pinning schemes for enhanced superconducting property in high temperature superconductor YBa <sub>2</sub> Cu <sub>3</sub> O <sub>7â^'<i>x</i></sub> : a review. Superconductor Science and Technology, 2017, 30, 114004.	3.5	19
375	Real-Time and Label-Free Chemical Sensor-on-a-chip using Monolithic Si-on-BaTiO3 Mid-Infrared waveguides. Scientific Reports, 2017, 7, 5836.	3.3	19
376	Coupled solute effects enable anomalous high-temperature strength and stability in nanotwinned Al alloys. Acta Materialia, 2020, 200, 378-388.	7.9	19
377	Tunable, room-temperature multiferroic Fe-BaTiO3 vertically aligned nanocomposites with perpendicular magnetic anisotropy. Materials Today Nano, 2020, 11, 100083.	4.6	19
378	Benefits of current percolation in superconducting coated conductors. Applied Physics Letters, 2005, 87, 162507.	3.3	18

#	Article	IF	CITATIONS
379	The role of a ZnO buffer layer in the growth of ZnO thin film on Al2O3 substrate. Superlattices and Microstructures, 2006, 40, 501-506.	3.1	18
380	Enhanced superconducting properties in epitaxial FeSe thin films with self-assembled Fe3O4 nanoparticles. Physica C: Superconductivity and Its Applications, 2011, 471, 515-519.	1.2	18
381	Four-fold Raman enhancement of 2D band in twisted bilayer graphene: evidence for a doubly degenerate Dirac band and quantum interference. Nanotechnology, 2014, 25, 335201.	2.6	18
382	Ferroelectric Sm-Doped BiMnO <sub>3</sub> Thin Films with Ferromagnetic Transition Temperature Enhanced to 140 K. ACS Applied Materials & Interfaces, 2014, 6, 14836-14843.	8.0	18
383	Comparison of temperature dependent deformation mechanisms of 8YSZ thermal barrier coatings prepared by air-plasma-spray and D-gun thermal spray: An in situ study. Journal of the European Ceramic Society, 2019, 39, 3120-3128.	5.7	18
384	Enhancing electrochemical performance of thin film lithium ion battery via introducing tilted metal nanopillars as effective current collectors. Nano Energy, 2020, 69, 104381.	16.0	18
385	3D Hybrid Plasmonic Framework with Au Nanopillars Embedded in Nitride Multilayers Integrated on Si. Advanced Materials Interfaces, 2020, 7, 2000493.	3.7	18
386	Self-biased magnetoelectric switching at room temperature in three-phase ferroelectric–antiferromagnetic–ferrimagnetic nanocomposites. Nature Electronics, 2021, 4, 333-341.	26.0	18
387	Printing dynamic color palettes and layered textures through modeling-guided stacking of electrochromic polymers. Materials Horizons, 2022, 9, 425-432.	12.2	18
388	Effects of the Variable Lorentz Force on the Critical Current in Anisotropic Superconducting Thin Films. IEEE Transactions on Applied Superconductivity, 2007, 17, 3697-3700.	1.7	17
389	Amorphous Silica Nanoparticles Embedded in Epitaxial SrTiO <sub>3</sub> and CoFe <sub>2</sub> O <sub>4</sub> Matrices. Angewandte Chemie - International Edition, 2008, 47, 5768-5771.	13.8	17
390	Microstructural and Pinning Properties of \${m YBa}_{2}{m Cu}_{3}{m O}_{7-delta}\$ Thin Films Doped With Magnetic Nanoparticles. IEEE Transactions on Applied Superconductivity, 2009, 19, 3503-3506.	1.7	17
391	Understanding nanoparticle self-assembly for a strong improvement in functionality in thin film nanocomposites. Nanotechnology, 2010, 21, 095604.	2.6	17
392	Microstructural and electrical properties of Ce <sub>0.9</sub> Gd <sub>0.1</sub> O <sub>1.95</sub> thin-film electrolyte in solid-oxide fuel cells. Journal of Materials Research, 2011, 26, 854-859.	2.6	17
393	Room temperature mechanical behaviour of a Ni-Fe multilayered material with modulated grain size distribution. Philosophical Magazine, 2014, 94, 3549-3559.	1.6	17
394	Tailoring plasticity of metallic glasses via interfaces in Cu/amorphous CuNb laminates. Journal of Materials Research, 2017, 32, 2680-2689.	2.6	17
395	In Situ Studies on Twin-Thickness-Dependent Distribution of Defect Clusters in Heavy Ion-Irradiated Nanotwinned Ag. Metallurgical and Materials Transactions A: Physical Metallurgy and Materials Science, 2017, 48, 1466-1473.	2.2	17
396	In situ study on enhanced heavy ion irradiation tolerance of porous Mg. Scripta Materialia, 2018, 144, 13-17.	5.2	17

#	Article	IF	CITATIONS
397	Strain Enhanced Functionality in a Bottomâ€Up Approach Enabled 3D Superâ€Nanocomposites. Advanced Functional Materials, 2019, 29, 1900442.	14.9	17
398	Multifunctional self-assembled BaTiO3-Au nanocomposite thin films on flexible mica substrates with tunable optical properties. Applied Materials Today, 2020, 21, 100856.	4.3	17
399	Nanoengineering room temperature ferroelectricity into orthorhombic SmMnO3 films. Nature Communications, 2020, 11, 2207.	12.8	17
400	Microstructure and tensile behavior of nanostructured gradient TWIP steel. Materials Science & Engineering A: Structural Materials: Properties, Microstructure and Processing, 2020, 785, 139346.	5.6	17
401	Design of 3D Oxide–Metal Hybrid Metamaterial for Tailorable Light–Matter Interactions in Visible and Nearâ€Infrared Region. Advanced Optical Materials, 2021, 9, .	7.3	17
402	High-Temperature and Flexible Piezoelectric Sensors for Lamb-Wave-Based Structural Health Monitoring. ACS Applied Materials & Interfaces, 2021, 13, 47764-47772.	8.0	17
403	Origins of stored enthalpy in cryomilled nanocrystalline Zn. Journal of Materials Research, 2001, 16, 3485-3495.	2.6	16
404	Critical factors that determine face-centered cubic to body-centered cubic phase transformation in sputter-deposited austenitic stainless steel films. Journal of Materials Research, 2004, 19, 1696-1702.	2.6	16
405	Characteristics of Alumina Diffusion Barrier Films on Hastelloy. Journal of Materials Research, 2004, 19, 1175-1180.	2.6	16
406	Growth of high-quality carbon nanotubes on free-standing diamond substrates. Carbon, 2010, 48, 2442-2446.	10.3	16
407	Enhanced flux pinning properties in superconducting FeSe <sub>0.5</sub> Te <sub>0.5</sub> thin films with secondary phases. Superconductor Science and Technology, 2012, 25, 025020.	3.5	16
408	Significant enhancement in the thermal stability of nanocrystalline metals via immiscible tri-phases. Scripta Materialia, 2012, 67, 177-180.	5.2	16
409	Superior power density solid oxide fuel cells by enlarging the three-phase boundary region of a NiO–Ce0.8Gd0.2O1.9 composite anode through optimized surface structure. Physical Chemistry Chemical Physics, 2013, 15, 14966.	2.8	16
410	Enhanced Flux Pinning Properties in Self-Assembled Magnetic \$hbox{CoFe}_{2}hbox{O}_{4}\$ Nanoparticles Doped \$ hbox{YBa}_{2}hbox{Cu}_{3}hbox{O}_{7 - delta}\$ Thin Films. IEEE Transactions on Applied Superconductivity, 2013, 23, 8001204-8001204.	1.7	16
411	Enhancement of Low-field Magnetoresistance in Self-Assembled Epitaxial La0.67Ca0.33MnO3:NiO and La0.67Ca0.33MnO3:Co3O4 Composite Films via Polymer-Assisted Deposition. Scientific Reports, 2016, 6, 26390.	3.3	16
412	Plastic deformation in nanocrystalline TiN at ultra-low stress: An in situ nanoindentation study. Materials Science & Engineering A: Structural Materials: Properties, Microstructure and Processing, 2016, 650, 445-453.	5.6	16
413	Tunable magnetic anisotropy of self-assembled Fe nanostructures within a La0.5Sr0.5FeO3 matrix. Applied Physics Letters, 2018, 112, .	3.3	16
414	Oxygen-vacancy-mediated dielectric property in perovskite Eu0.5Ba0.5TiO3-δ epitaxial thin films. Applied Physics Letters, 2018, 112, .	3.3	16

#	Article	IF	CITATIONS
415	All-Oxide Nanocomposites to Yield Large, Tunable Perpendicular Exchange Bias above Room Temperature. ACS Applied Materials & Interfaces, 2018, 10, 42593-42602.	8.0	16
416	Staged microstructural study of flash sintered titania. Materialia, 2019, 8, 100451.	2.7	16
417	Strain and property tuning of the 3D framed epitaxial nanocomposite thin films via interlayer thickness variation. Journal of Applied Physics, 2019, 125, .	2.5	16
418	Au-Encapsulated Fe Nanorods in Oxide Matrix with Tunable Magneto-Optic Coupling Properties. ACS Applied Materials & Interfaces, 2020, 12, 51827-51836.	8.0	16
419	Microstructural evolution of nanotwinned Al-Zr alloy with significant 9R phase. Materials Research Letters, 2021, 9, 91-98.	8.7	16
420	Laser-induced atmospheric Cu <sub><i>x</i></sub> O formation on copper surface with enhanced electrochemical performance for non-enzymatic glucose sensing. Journal of Materials Chemistry C, 2021, 9, 14997-15010.	5.5	16
421	Electrochromic Properties of Perovskite NdNiO <sub>3</sub> Thin Films for Smart Windows. ACS Applied Electronic Materials, 2021, 3, 1719-1731.	4.3	16
422	Heavy ion irradiation response of an additively manufactured 316LN stainless steel. Journal of Nuclear Materials, 2021, 546, 152745.	2.7	16
423	A Biodegradable Hybrid Micro/Nano Conductive Zinc Paste for Paperâ€Based Flexible Bioelectronics. Advanced Materials Technologies, 2022, 7, .	5.8	16
424	Lateral epitaxial growth of (Ba,Sr)TiO3 thin films. Applied Physics Letters, 2003, 83, 5494-5496.	3.3	15
425	High critical current densities in YBa2Cu3O7â^'x films grown at high rates by hybrid liquid phase epitaxy. Applied Physics Letters, 2005, 87, 252507.	3.3	15
426	Ferroic metal-oxide films grown by polymer assisted deposition. Thin Solid Films, 2007, 515, 6411-6415.	1.8	15
427	Epitaxial GaN Thin Films Prepared by Polymer-Assisted Deposition. Journal of Physical Chemistry C, 2008, 112, 20535-20538.	3.1	15
428	Microstructure and electrochemical properties of PrBaCo2O5+Î′/Ce0.9Gd0.1O1.95 vertically aligned nanocomposite thin film as interlayer for thin film solid oxide fuel cells. Electrochimica Acta, 2012, 62, 147-152.	5.2	15
429	Manipulating leakage behavior via distribution of interfaces in oxide thin films. Applied Physics Letters, 2014, 105, 072907.	3.3	15
430	Strong correlated pinning at high growth rates in YBa2Cu3O7â^'x thin films with Ba2YNbO6 additions. Journal of Applied Physics, 2014, 116, .	2.5	15
431	Tunable flux pinning landscapes achieved by functional ferromagnetic Fe2O3:CeO2 vertically aligned nanocomposites in YBa2Cu3O7â^îî´thin films. Physica C: Superconductivity and Its Applications, 2015, 510, 13-20.	1.2	15
432	Strongly Biasâ€Dependent Tunnel Magnetoresistance in Manganite Spin Filter Tunnel Junctions. Advanced Materials, 2015, 27, 3079-3084.	21.0	15

#	Article	IF	CITATIONS
433	xmlns:mml="http://www.w3.org/1998/Math/MathML"> <mml:mrow><mml:mi mathvariant="normal"&gt;E<mml:msub><mml:mi mathvariant="normal"&gt;u<mml:mrow><mml:mn>0.5</mml:mn></mml:mrow></mml:mi </mml:msub><mml:mi mathvariant="normal"&gt;B<mml:msub><mml:mi< td=""><td>3.2</td><td>15</td></mml:mi<></mml:msub></mml:mi </mml:mi </mml:mrow>	3.2	15
434	mathvariant="normal">a <mml:mrow><mml:mn>0.5</mml:mn></mml:mrow> <mml:mi>Ti Strengthening mechanisms and deformability of nanotwinned AlMg alloys. Journal of Materials Research, 2018, 33, 3739-3749.</mml:mi>	i2.6	> < mml:msul 15
435	Tunable low-field magnetoresistance properties in (La0.7Ca0.3MnO3)1â^'x:(CeO2)x vertically aligned nanocomposite thin films. Applied Physics Letters, 2019, 115, 053103.	3.3	15
436	Tuning magnetic anisotropy in Co–BaZrO <sub>3</sub> vertically aligned nanocomposites for memory device integration. Nanoscale Advances, 2019, 1, 4450-4458.	4.6	15
437	Study of BaCe0.4Zr0.4Y0.2O3-δ/BaCe0.8Pr0.2O3-δ (BCZY/BCP) bilayer membrane for Protonic Conductor Solid Oxide Fuel Cells (PC-SOFC). International Journal of Hydrogen Energy, 2020, 45, 5481-5490.	7.1	15
438	Induced ferroelectric phases in SrTiO <sub>3</sub> by a nanocomposite approach. Nanoscale, 2020, 12, 18193-18199.	5.6	15
439	Vertically aligned nanocomposite (BaTiO <sub>3</sub> ) <sub>0.8</sub> : (La <sub>0.7</sub> Sr <sub>0.3</sub> MnO <sub>3</sub> ) <sub> thin films with anisotropic multifunctionalities. Nanoscale Advances, 2020, 2, 3276-3283.</sub>	042x/sub>	15
440	Thermally Stable Au–BaTiO <sub>3</sub> Nanoscale Hybrid Metamaterial for High-Temperature Plasmonic Applications. ACS Applied Nano Materials, 2020, 3, 1431-1437.	5.0	15
441	Ferroelectric/multiferroic self-assembled vertically aligned nanocomposites: Current and future status. APL Materials, 2021, 9, .	5.1	15
442	Heteroepitaxy of flexible piezoelectric Pb(Zr0.53Ti0.47)O3 sensor on inorganic mica substrate for lamb wave-based structural health monitoring. Ceramics International, 2021, 47, 13156-13163.	4.8	15
443	Microstructural Evolution With the Change in Thickness of Superconducting Films. IEEE Transactions on Applied Superconductivity, 2007, 17, 3243-3246.	1.7	14
444	Spontaneous Ordering, Strain Control, and Multifunctionality in Vertical Nanocomposite Heteroepitaxial Films. IEEE Transactions on Ultrasonics, Ferroelectrics, and Frequency Control, 2009, 56, 1534-1538.	3.0	14
445	Flux Pinning Properties in YBCO Thin Films With Self-Aligned Magnetic Nanoparticles. IEEE Transactions on Applied Superconductivity, 2011, 21, 2749-2752.	1.7	14
446	Interfacial defects distribution and strain coupling in the vertically aligned nanocomposite YBa <sub>2</sub> Cu <sub>3</sub> O <sub>7-X</sub> / BaSnO <sub>3</sub> thin films. Journal of Materials Research, 2012, 27, 1763-1769.	2.6	14
447	Microstructure and superconducting properties of YBa <sub>2</sub> Cu <sub>3</sub> O <sub>7â^î^</sub> thin films incorporated with a self-assembled magnetic vertically aligned nanocomposite. Superconductor Science and Technology, 2012, 25, 075016.	3.5	14
448	In situ studies on superior thermal stability of bulk FeZr nanocomposites. Acta Materialia, 2015, 101, 125-135.	7.9	14
449	Measurement of Heavy Ion Irradiation Induced In-Plane Strain in Patterned Face-Centered-Cubic Metal Films: An <i>in Situ</i> Study. Nano Letters, 2016, 16, 7481-7489.	9.1	14
450	Upper Critical Field and Kondo Effects in Fe(Te0.9Se0.1) Thin Films by Pulsed Field Measurements. Scientific Reports, 2016, 6, 21469.	3.3	14

#	Article	IF	CITATIONS
451	In Situ Nanoindentation Studies on Detwinning and Work Hardening in Nanotwinned Monolithic Metals. Jom, 2016, 68, 127-135.	1.9	14
452	<i>In situ</i> study on surface roughening in radiation-resistant Ag nanowires. Nanotechnology, 2018, 29, 215708.	2.6	14
453	A Review on the Radiation Response of Nanoporous Metallic Materials. Jom, 2018, 70, 2753-2764.	1.9	14
454	In-situ high temperature micromechanical testing of ultrafine grained yttria-stabilized zirconia processed by spark plasma sintering. Acta Materialia, 2018, 155, 128-137.	7.9	14
455	Multiferroic vertically aligned nanocomposite with CoFe2O4 nanocones embedded in layered Bi2WO6 matrix. Materials Research Letters, 2019, 7, 418-425.	8.7	14
456	Self-assembled two-dimensional layered oxide supercells with modulated layer stacking and tunable physical properties. Materials Today Nano, 2019, 6, 100037.	4.6	14
457	An in situ study on Kr ion–irradiated crystalline Cu/amorphous-CuNb nanolaminates. Journal of Materials Research, 2019, 34, 2218-2228.	2.6	14
458	In-situ studies on the mechanical properties of He ion irradiated nanotwinned Ag. Journal of Nuclear Materials, 2020, 540, 152392.	2.7	14
459	Morphology Control of Self-Assembled Three-Phase Au-BaTiO <sub>3</sub> –ZnO Hybrid Metamaterial for Tunable Optical Properties. Crystal Growth and Design, 2020, 20, 6101-6108.	3.0	14
460	Vertical Strain-Driven Antiferromagnetic to Ferromagnetic Phase Transition in EuTiO <sub>3</sub> Nanocomposite Thin Films. ACS Applied Materials & Interfaces, 2020, 12, 8513-8521.	8.0	14
461	Effects of electric field on microstructure evolution and defect formation in flash-sintered TiO2. Journal of the European Ceramic Society, 2022, 42, 6040-6047.	5.7	14
462	Growth and characteristics of TaN/TiN superlattice structures. Applied Physics Letters, 2003, 83, 3072-3074.	3.3	13
463	Cubic TaN diffusion barrier for Cu interconnects using an ultra-thin TiN seed layer. Thin Solid Films, 2008, 516, 5103-5106.	1.8	13
464	Self-separated PZT thick films with bulk-like piezoelectric and electromechanical properties. Journal of Materials Research, 2011, 26, 1431-1435.	2.6	13
465	In situ nanomechanical testing of twinned metals in a transmission electron microscope. MRS Bulletin, 2016, 41, 305-313.	3.5	13
466	Dual Beam In Situ Radiation Studies of Nanocrystalline Cu. Materials, 2019, 12, 2721.	2.9	13
467	Integration of highly anisotropic multiferroic BaTiO3–Fe nanocomposite thin films on Si towards device applications. Nanoscale Advances, 2020, 2, 4172-4178.	4.6	13
468	Bidirectional tuning of phase transition properties in Pt : VO <sub>2</sub> nanocomposite thin films. Nanoscale, 2020, 12, 17886-17894.	5.6	13

#	Article	IF	CITATIONS
469	Formation of liquid phase and nanostructures in flash sintered ZnO. Scripta Materialia, 2021, 195, 113719.	5.2	13
470	Ultra-high heating rate effects on the sintering of ceramic nanoparticles: an <i>inÂsitu</i> TEM study. Materials Research Letters, 2021, 9, 373-381.	8.7	13
471	High-strength nanocrystalline intermetallics with room temperature deformability enabled by nanometer thick grain boundaries. Science Advances, 2021, 7, .	10.3	13
472	Laser-Assisted Nanotexturing and Silver Immobilization on Titanium Implant Surfaces to Enhance Bone Cell Mineralization and Antimicrobial Properties. Langmuir, 2022, 38, 4014-4027.	3.5	13
473	Thickness dependence of ac losses in circular disks of YBa2Cu3O7 films in perpendicular magnetic fields. Journal of Applied Physics, 2004, 95, 208-213.	2.5	12
474	Nanoporous thin films with controllable nanopores processed from vertically aligned nanocomposites. Nanotechnology, 2010, 21, 285606.	2.6	12
475	Biopolymer mediated synthesis of plate-like YBCO with enhanced grain connectivity and intragranular critical current. CrystEngComm, 2012, 14, 5765.	2.6	12
476	Effects of interlayer thickness on the electrochemical and mechanical properties of bi-layer cathodes for solid oxide fuel cells. Journal of Power Sources, 2012, 218, 261-267.	7.8	12
477	Magnetic field induced phase transformation in polycrystalline NiCoMnAl thin films. Applied Physics Letters, 2013, 103, 132404.	3.3	12
478	Strain dependent ultrafast carrier dynamics in EuTiO3 films. Applied Physics Letters, 2014, 105, .	3.3	12
479	Photoluminescence study of p-type vs. n-type Ag-doped ZnO films. Journal of Applied Physics, 2015, 118, .	2.5	12
480	Defect evolution in heavy ion irradiated nanotwinned Cu with nanovoids. Journal of Nuclear Materials, 2017, 496, 293-300.	2.7	12
481	Atomicâ€Scale Control of Electronic Structure and Ferromagnetic Insulating State in Perovskite Oxide Superlattices by Longâ€Range Tuning of BO <sub>6</sub> Octahedra. Advanced Functional Materials, 2020, 30, 2001984.	14.9	12
482	Design of super-strong and thermally stable nanotwinned Al alloys <i>via</i> solute synergy. Nanoscale, 2020, 12, 20491-20505.	5.6	12
483	Self-assembled nitride–metal nanocomposites: recent progress and future prospects. Nanoscale, 2020, 12, 20564-20579.	5.6	12
484	Dipotassium terephthalate as promising potassium storing anode with DFT calculations. Materials Today Energy, 2020, 17, 100454.	4.7	12
485	Achieving ferromagnetic insulating properties in La <sub>0.9</sub> Ba <sub>0.1</sub> MnO <sub>3</sub> thin films through nanoengineering. Nanoscale, 2020, 12, 9255-9265.	5.6	12
486	Selfâ€Assembled Metal–Dielectric Hybrid Metamaterials in Vertically Aligned Nanocomposite Form with Tailorable Optical Properties and Coupled Multifunctionalities. Advanced Photonics Research, 2021, 2, 2000174.	3.6	12

#	Article	IF	CITATIONS
487	Flash sintering of additively manufactured 3YSZ gears. Journal of the American Ceramic Society, 2021, 104, 3828-3832.	3.8	12
488	Enhancing magnetic pinning by BaZrO <sub>3</sub> nanorods forming coherent interface by strain-directed Ca-doping in YBa <sub>2</sub> Cu <sub>3</sub> O <sub>7â^'x</sub> nanocomposite films. Superconductor Science and Technology, 2021, 34, 104002.	3.5	12
489	Microstructure and defect gradients in DC and AC flash sintered ZnO. Ceramics International, 2021, 47, 28596-28602.	4.8	12
490	Temperature and Magnetic Field Dependence of Critical Current Density of YBCO With Varying Flux Pinning Additions. IEEE Transactions on Applied Superconductivity, 2009, 19, 3270-3274.	1.7	11
491	High current, low cost YBCO conductors—what's next?. Superconductor Science and Technology, 2010, 23, 034009.	3.5	11
492	Enhanced electrochemical properties of Bi-layer La0.5Sr0.5CoO3â^'δ cathode prepared by a hybrid method. Electrochimica Acta, 2011, 56, 3969-3974.	5.2	11
493	Influence of SrTiO3 substrate miscut angle on the transport properties of LaAlO3/SrTiO3 interfaces. Applied Physics Letters, 2011, 99, .	3.3	11
494	Aligned carbon nanotubes sandwiched in epitaxial NbC film for enhanced superconductivity. Nanoscale, 2012, 4, 2268.	5.6	11
495	Atomic interface sequence, misfit strain relaxation and intrinsic flux-pinning defects in different YBa <sub>2</sub> Cu <sub>3</sub> O <sub>7â^´Î´</sub> heterogeneous systems. Superconductor Science and Technology, 2013, 26, 025009.	3.5	11
496	Atomic-Scale Investigations of Intrinsic Chemical Inhomogeneity in Superconducting Fe <sub>1+<i>y</i></sub> Se <sub>1–<i>x</i></sub> Te <sub><i>x</i></sub> Epitaxial Films. Journal of Physical Chemistry C, 2013, 117, 7170-7177.	3.1	11
497	Thermal stability of amorphous SiOC/crystalline Fe composite. Philosophical Magazine, 2015, 95, 3876-3887.	1.6	11
498	Room temperature magnetodielectric effects in epitaxial hexaferrite BaFe10.2Sc1.8O19 thin film. Applied Physics Letters, 2017, 110, .	3.3	11
499	Li <sub>2</sub> MnO <sub>3</sub> Thin Films with Tilted Domain Structure as Cathode for Li-Ion Batteries. ACS Applied Energy Materials, 2019, 2, 3461-3468.	5.1	11
500	Radiation induced nanovoid shrinkage in Cu at room temperature: An in situ study. Scripta Materialia, 2019, 166, 112-116.	5.2	11
501	Fieldâ€assisted heating of Gdâ€doped ceria thin film. Journal of the American Ceramic Society, 2020, 103, 2309-2314.	3.8	11
502	Irradiation induced void spheroidization, shrinkage and migration in Cu at elevated temperatures: An in situ study. Acta Materialia, 2020, 201, 504-516.	7.9	11
503	Anisotropic domains and antiferrodistortive-transition controlled magnetization in epitaxial manganite films on vicinal SrTiO3 substrates. Applied Physics Letters, 2020, 117, .	3.3	11
504	Negative-pressure enhanced ferroelectricity and piezoelectricity in lead-free BaTiO <sub>3</sub> ferroelectric nanocomposite films. Journal of Materials Chemistry C, 2020, 8, 8091-8097.	5.5	11

#	Article	IF	CITATIONS
505	Novel layered Bi <sub>3</sub> MoM <sub>T</sub> O <sub>9</sub> (M <sub>T</sub> = Mn, Fe, Co and Ni) thin films with tunable multifunctionalities. Nanoscale, 2020, 12, 5914-5921.	5.6	11
506	Largeâ€6cale Plasmonic Hybrid Framework with Builtâ€In Nanohole Array as Multifunctional Optical Sensing Platforms. Small, 2020, 16, 1906459.	10.0	11
507	Electric field-induced grain boundary degradation mechanism in yttria stabilized zirconia. Scripta Materialia, 2021, 204, 114130.	5.2	11
508	Freestanding La <sub>0.7</sub> Sr <sub>0.3</sub> MnO <sub>3</sub> :NiO vertically aligned nanocomposite thin films for flexible perpendicular interfacial exchange coupling. Materials Research Letters, 2022, 10, 287-294.	8.7	11
509	TaN-TiN binary alloys and superlattices as diffusion barriers for copper interconnects. Journal of Electronic Materials, 2003, 32, 994-999.	2.2	10
510	Formation of misfit dislocations in strained-layer GaAs/In[sub x]Ga[sub 1â^'x]As/GaAs heterostructures during postfabrication thermal processing. Journal of Applied Physics, 2003, 94, 7496.	2.5	10
511	Magnetotransport properties of Pr0.5Ca0.5MnO3 thin films grown by a solution route. Journal of Applied Physics, 2011, 110, 013921.	2.5	10
512	Highly stable non-polar p-type Ag-doped ZnO thin films grown on r-cut sapphire. Materials Letters, 2013, 100, 78-81.	2.6	10
513	Repetitive Ultra-low Stress Induced Nanocrystallization in Amorphous Cu‒Zr‒Al Alloy Evidenced byin situNanoindentation. Materials Research Letters, 2014, 2, 209-216.	8.7	10
514	In situ neutron diffraction study on temperature dependent deformation mechanisms of ultrafine grained austenitic Fe–14Cr–16Ni alloy. International Journal of Plasticity, 2014, 53, 125-134.	8.8	10
515	Nanostructured pinning centers in FeSe0.1Te0.9thin films for enhanced superconducting properties. Superconductor Science and Technology, 2014, 27, 105006.	3.5	10
516	Deformation behavior of multilayered NiFe with bimodal grain size distribution at room and elevated temperature. Materials Science & Engineering A: Structural Materials: Properties, Microstructure and Processing, 2016, 656, 174-183.	5.6	10
517	Giant Enhancement of Polarization and Strong Improvement of Retention in Epitaxial Ba <sub>0.6</sub> Sr <sub>0.4</sub> TiO <sub>3</sub> â€Based Nanocomposites. Advanced Materials Interfaces, 2017, 4, 1700336.	3.7	10
518	Use of Mesoscopic Host Matrix to Induce Ferrimagnetism in Antiferromagnetic Spinel Oxide. Advanced Functional Materials, 2018, 28, 1706220.	14.9	10
519	Tunable physical properties in BiAl <sub>1â^'x</sub> Mn <sub>x</sub> O <sub>3</sub> thin films with novel layered supercell structures. Nanoscale Advances, 2020, 2, 315-322.	4.6	10
520	Substrate oxygen sponge effect: A parameter for epitaxial manganite thin film growth. Applied Physics Letters, 2020, 117, .	3.3	10
521	Engineering lithium-ion battery cathodes for high-voltage applications using electromagnetic excitation. Journal of Materials Science, 2020, 55, 12177-12190.	3.7	10
522	Tailoring the formation of twins in Al by introducing epitaxial layer interfaces. Scripta Materialia, 2021, 192, 1-6.	5.2	10

#	Article	IF	CITATIONS
523	Epitaxial TiN/MgO multilayers with ultrathin TiN and MgO layers as hyperbolic metamaterials in visible region. Materials Today Physics, 2021, 16, 100316.	6.0	10
524	High performance, electroforming-free, thin film memristors using ionic Na <sub>0.5</sub> Bi <sub>0.5</sub> TiO <sub>3</sub> . Journal of Materials Chemistry C, 2021, 9, 4522-4531.	5.5	10
525	Ultrathin epitaxial NbN superconducting films with high upper critical field grown at low temperature. Materials Research Letters, 2021, 9, 336-342.	8.7	10
526	High stability of flexible perovskite transparent conductive oxide film via van der Waals heteroepitaxy. Journal of Alloys and Compounds, 2022, 890, 161897.	5.5	10
527	Effects of incubation on microstructure gradient in flash-sintered TiO2. Scripta Materialia, 2022, 207, 114270.	5.2	10
528	High ionic conductivity in fluorite δ-bismuth oxide-based vertically aligned nanocomposite thin films. Journal of Materials Chemistry A, 2022, 10, 3478-3484.	10.3	10
529	Role of Defects and Power Dissipation on Ferroelectric Memristive Switching. Advanced Electronic Materials, 2022, 8, .	5.1	10
530	Study of \${m Sm}_{m x}{m Zr}_{1-{m x}}{m O}_{m y}\$ Buffer Layer and Its Effects on YBCO Properties. IEEE Transactions on Applied Superconductivity, 2007, 17, 3409-3412.	1.7	9
531	Cubic HfN Thin Films with Low Resistivity on Si (001) and MgO (001) Substrates. Journal of Electronic Materials, 2008, 37, 1828-1831.	2.2	9
532	Correlation Between Flux Pinning Properties and Interfacial Defects in \${m YBa}_{2}{m Cu}_{3}{m O}_{7-delta}/{m CeO}_{2}\$ Multilayer Thin Films. IEEE Transactions on Applied Superconductivity, 2011, 21, 2758-2761.	1.7	9
533	Magnetic (CoFe2O4)0.1(CeO2)0.9nanocomposite as effective pinning centers in FeSe0.1Te0.9thin films. Journal of Physics Condensed Matter, 2016, 28, 025702.	1.8	9
534	3D Hybrid Trilayer Heterostructure: Tunable Au Nanorods and Optical Properties. ACS Applied Materials & Interfaces, 2020, 12, 45015-45022.	8.0	9
535	Origin of unexpected lattice expansion and ferromagnetism in epitaxial EuTiO3â€"î´ thin films. Ceramics International, 2020, 46, 19990-19995.	4.8	9
536	High-strength and tunable plasticity in sputtered Al–Cr alloys with multistage phase transformations. International Journal of Plasticity, 2021, 137, 102915.	8.8	9
537	Route to High-Performance Micro-solid Oxide Fuel Cells on Metallic Substrates. ACS Applied Materials & Interfaces, 2021, 13, 4117-4125.	8.0	9
538	Novel vertically aligned nanocomposite of Bi2WO6-Co3O4 with room-temperature multiferroic and anisotropic optical response. Nano Research, 0, , 1.	10.4	9
539	High Strength and Low Coercivity of Cobalt with Three-Dimensional Nanoscale Stacking Faults. Nano Letters, 2021, 21, 6480-6486.	9.1	9
540	Synthesis and Characterization of Cu-Doped <tex>\$rm SrTiO_3\$</tex> Powders and Sol-Gel Processed Buffer Layers on IBAD MgO Templates. IEEE Transactions on Applied Superconductivity, 2005, 15, 2703-2706.	1.7	8

#	Article	IF	CITATIONS
541	Thermal stability of sputtered Cuâ^•304 stainless steel multilayer films. Journal of Applied Physics, 2007, 101, 124311.	2.5	8
542	Attenuation of interfacial pinning enhancement in YBCO using a PrBCO buffer layer. Physica C: Superconductivity and Its Applications, 2009, 469, 2033-2036.	1.2	8
543	Highly Textured Superconducting FeSe0.5Te0.5Thin Films on Glass Substrates. Japanese Journal of Applied Physics, 2013, 52, 020201.	1.5	8
544	Stabilizing new bismuth compounds in thin film form. Journal of Materials Research, 2016, 31, 3530-3537.	2.6	8
545	Superconducting Iron Chalcogenide Thin Films Integrated on Flexible Mica Substrates. IEEE Transactions on Applied Superconductivity, 2019, 29, 1-4.	1.7	8
546	Breaking Lattice Symmetry in Highly Strained Epitaxial VO <sub>2</sub> Films on Faceted Nanosurface. ACS Applied Materials & Interfaces, 2019, 11, 44905-44912.	8.0	8
547	Recent Studies on Void Shrinkage in Metallic Materials Subjected to In Situ Heavy Ion Irradiations. Jom, 2020, 72, 4008-4016.	1.9	8
548	Self-Assembled BaTiO <sub>3</sub> –Au <i><sub>x</sub></i> Ag <sub>1–<i>x</i></sub> Low-Loss Hybrid Plasmonic Metamaterials with an Ordered "Nano-Domino-like―Microstructure. ACS Applied Materials & Interfaces, 2021, 13, 5390-5398.	8.0	8
549	Electrical properties and charge compensation mechanisms of Cr-doped rutile, TiO <sub>2</sub> . Physical Chemistry Chemical Physics, 2021, 23, 22133-22146.	2.8	8
550	Strong pinning at high growth rates in rare earth barium cuprate (REBCO) superconductor films grown with liquid-assisted processing (LAP) during pulsed laser deposition. Superconductor Science and Technology, 2021, 34, 045012.	3.5	8
551	Nanocompositeâ€ <del>S</del> eeded Epitaxial Growth of Singleâ€Domain Lithium Niobate Thin Films for Surface Acoustic Wave Devices. Advanced Photonics Research, 2021, 2, 2000149.	3.6	8
552	Field-assisted growth of one-dimensional ZnO nanostructures with high defect density. Nanotechnology, 2021, 32, 095603.	2.6	8
553	Electroforming-Free HfO <sub>2</sub> :CeO <sub>2</sub> Vertically Aligned Nanocomposite Memristors with Anisotropic Dielectric Response. ACS Applied Electronic Materials, 2021, 3, 5278-5286.	4.3	8
554	Enabling coherent BaZrO <sub>3</sub> nanorods/YBa <sub>2</sub> Cu <sub>3</sub> O <sub>7â^'x</sub> interface through dynamic lattice enlargement in vertical epitaxy of BaZrO <sub>3</sub> /YBa <sub>2</sub> Cu <sub>3</sub> O <sub>7â^'x</sub> nanocomposites.	3.5	8
555	Superconductor Science and Technology, 2022, 35, 034001. Preparation and characterization of multifunctional piezoenergetic polyvinylidene fluoride/aluminum nanocomposite films. Journal of Applied Physics, 2022, 131, .	2.5	8
556	Surface chemistry and porosity engineering through etching reveal ultrafast oxygen reduction kinetics below 400°C in B-site exposed (La,Sr)(Co,Fe)O3 thin-films. Journal of Power Sources, 2022, 523, 230983.	7.8	8
557	Microstructure and electronic properties of Cu/Mo multilayers and three-dimensional arrays of nanocrystalline Cu precipitates embedded in a Mo matrix. Journal of Applied Physics, 2004, 95, 3644-3648.	2.5	7
558	BaTiO <sub>3</sub> -RELATED FERROELECTRIC THIN FILMS BY POLYMER ASSISTED DEPOSITION. Integrated Ferroelectrics, 2008, 100, 132-139.	0.7	7

#	Article	IF	CITATIONS
559	A magnetic field sensitive interfacial metallic state in a crystalline insulator. Nanotechnology, 2008, 19, 305401.	2.6	7
560	Epitaxial cubic HfN diffusion barriers deposited on Si (001) by using a TiN buffer layer. Journal of Vacuum Science & Technology B, 2008, 26, 1871-1874.	1.3	7
561	Thermal diffusivity measurement of YBa2Cu3O7â^'x thin film with a picosecond thermoreflectance technique. Physica C: Superconductivity and Its Applications, 2010, 470, 365-368.	1.2	7
562	Growth of Al-doped ZnO films with tilted nano-columns on r-cut sapphire substrates by pulsed laser deposition. Thin Solid Films, 2012, 524, 320-327.	1.8	7
563	Enhanced Flux Pinning Properties of YBCO Thin Films With Various Pinning Landscapes. IEEE Transactions on Applied Superconductivity, 2017, 27, 1-5.	1.7	7
564	Investigation of KBiFe2O5 as a Photovoltaic Absorber. ACS Applied Energy Materials, 2019, 2, 8039-8044.	5.1	7
565	Comparison Study of the Flux Pinning Enhancement of YBa <sub>2</sub> Cu <sub>3</sub> O <sub>7â<sup>^</sup>î</sub> Thin Films With BaHfO <sub>3</sub> + Y <sub>2</sub> O <sub>3</sub> Single- and Mixed-Phase Additions. IEEE Transactions on Applied Superconductivity. 2019. 29. 1-5.	1.7	7
566	Optical and electrical properties of (111)-oriented epitaxial SrVO3 thin films. Ceramics International, 2019, 45, 11304-11308.	4.8	7
567	Titanium Nitride Modified Photoluminescence from Single Semiconductor Nanoplatelets. Advanced Functional Materials, 2020, 30, 1904179.	14.9	7
568	Ceramic Material Processing Towards Future Space Habitat: Electric Current-Assisted Sintering of Lunar Regolith Simulant. Materials, 2020, 13, 4128.	2.9	7
569	Role of Interlayer in 3D Vertically Aligned Nanocomposite Frameworks with Tunable Magnetotransport Properties. Advanced Materials Interfaces, 2020, 7, 1901990.	3.7	7
570	Ultra-high strength and plasticity mediated by partial dislocations and defect networks: Part II: Layer thickness effect. Acta Materialia, 2021, 204, 116494.	7.9	7
571	Deposition pressure-induced microstructure control and plasmonic property tuning in hybrid ZnO–Ag <sub>x</sub> Au <sub>1â^*x</sub> thin films. Nanoscale Advances, 2021, 3, 2870-2878.	4.6	7
572	Stress of misfit dislocation at Fe/MgO interface drives the annihilation of radiation induced defects. Acta Materialia, 2021, 210, 116798.	7.9	7
573	Strong Interfacial Coupling of Tunable Ni–NiO Nanocomposite Thin Films Formed by Self-Decomposition. ACS Applied Materials & Interfaces, 2021, 13, 39730-39737.	8.0	7
574	Deformation mechanism in nanolaminate FeCrAl alloys by in situ micromechanical strain rate jump tests at elevated temperatures. Scripta Materialia, 2022, 215, 114698.	5.2	7
575	Tunable Three-Phase Co–CeO <sub>2</sub> –BaTiO <sub>3</sub> Hybrid Metamaterials with Nano-Mushroom-Like Structure for Tailorable Multifunctionalities. ACS Applied Nano Materials, 2022, 5, 6297-6304.	5.0	7
576	Vertically stacked multilayer atomic-layer-deposited sub-1-nm In2O3 field-effect transistors with back-end-of-line compatibility. Applied Physics Letters, 2022, 120, .	3.3	7

#	Article	IF	CITATIONS
577	Tunable physical properties in Bi-based layered supercell multiferroics embedded with Au nanoparticles. Nanoscale Advances, 2022, 4, 3054-3064.	4.6	7
578	<tex>\$J_rm c(H)\$</tex> Crossover in YBCO Thick Films and Bi2223/Ag Tapes With Columnar Defects. IEEE Transactions on Applied Superconductivity, 2005, 15, 2787-2789.	1.7	6
579	Comparative Study of Microstructural Properties for YBa2Cu3O7 Films on Single-crystal and Ni-based Metal Substrates. Journal of Materials Research, 2005, 20, 2055-2060.	2.6	6
580	\${m YBa}_{2}{m Cu}_{3}{m O}_{7}\$ Coated Conductor Grown by Hybrid Liquid Phase Epitaxy. IEEE Transactions on Applied Superconductivity, 2007, 17, 2537-2541.	1.7	6
581	Interfacial Defects and Flux-Pinning Effects in Nanostructured \${m YBa}_{2}{m Cu}_{3}{m O}_{7-delta}\$ Thin Films. IEEE Transactions on Applied Superconductivity, 2009, 19, 3395-3398.	1.7	6
582	Highlc, YBa2Cu3O7â^'xfilms grown at very high rates by liquid assisted growth incorporating lightly Au-doped SrTiO3buffers. Superconductor Science and Technology, 2009, 22, 015009.	3.5	6
583	Growth and Pinning Properties of Superconducting Nanostructured \$hbox{FeSe}_{0.5}hbox{Te}_{0.5}\$ Thin Films on Amorphous Substrates. IEEE Transactions on Applied Superconductivity, 2013, 23, 7500904-7500904.	1.7	6
584	Superconducting properties of FeSexTe1â^'xthin film with a composition close to antiferromagnetic ordering. Superconductor Science and Technology, 2013, 26, 112001.	3.5	6
585	Superconducting FeSe <sub>0.1</sub> Te <sub>0.9</sub> thin films integrated on Si-based substrates. Journal Physics D: Applied Physics, 2018, 51, 205301.	2.8	6
586	Interfacial Engineering Enabled Novel Bi-Based Layered Oxide Supercells with Modulated Microstructures and Tunable Physical Properties. Crystal Growth and Design, 2019, 19, 7088-7095.	3.0	6
587	Defectâ€Mediated Anisotropic Lattice Expansion in Ceramics as Evidence for Nonthermal Coupling between Electromagnetic Fields and Matter. Advanced Engineering Materials, 2019, 21, 1900762.	3.5	6
588	AlN-based hybrid thin films with self-assembled plasmonic Au and Ag nanoinclusions. Applied Physics Letters, 2019, 114, .	3.3	6
589	Magnetic signatures of 120 K superconductivity at interfaces in La <sub>2</sub> CuO <sub>4+δ</sub> . Nanoscale, 2020, 12, 3157-3165.	5.6	6
590	Room-Temperature Ferroelectric LiNb <sub>6</sub> Ba <sub>5</sub> Ti <sub>4</sub> O <sub>30</sub> Spinel Phase in a Nanocomposite Thin Film Form for Nonlinear Photonics. ACS Applied Materials & Interfaces, 2020, 12, 23076-23083.	8.0	6
591	Double-Exchange Bias Modulation under Horizontal and Perpendicular Field Directions by 3D Nanocomposite Design. ACS Applied Materials & Interfaces, 2021, 13, 50141-50148.	8.0	6
592	Self-assembled vertically aligned nanocomposite systems integrated on silicon substrate: Progress and future perspectives. Journal of Vacuum Science and Technology A: Vacuum, Surfaces and Films, 2022, 40, .	2.1	6
593	Epitaxial (110)-oriented La <sub>0.7</sub> Sr <sub>0.3</sub> MnO <sub>3</sub> film directly on flexible mica substrate. Journal Physics D: Applied Physics, 2022, 55, 224002.	2.8	6
594	Lithium-based vertically aligned nancomposite films incorporating LixLa0.32(Nb0.7Ti0.32)O3 electrolyte with high Li+ ion conductivity. APL Materials, 2022, 10, .	5.1	6

#	Article	IF	CITATIONS
595	WEAK-LOCALIZATION EFFECT IN SINGLE CRYSTAL TaN(001) FILMS. Modern Physics Letters B, 2002, 16, 1143-1149.	1.9	5
596	Synthesis and ferroelectric properties of SrBi2Ta2O9/Bi4Ti3O12/p-Si multilayer thin films by Sol-Gel. Journal of Materials Science: Materials in Electronics, 2006, 17, 165-169.	2.2	5
597	High \$I_{m c}\$ in YBCO Films Grown at Very High Rates by Liquid Mediated Growth. IEEE Transactions on Applied Superconductivity, 2009, 19, 3180-3183.	1.7	5
598	Microstructural and electrical properties of Ce <sub>0.9</sub> Gd <sub>0.101.95</sub> thin film electrolyte in solid oxide fuel cells – CORRIGENDUM. Journal of Materials Research, 2011, 26, 1.	2.6	5
599	Direct observation of twin deformation in YBa2Cu3O7â^' <i>x</i> thin films by <i>in situ</i> nanoindentation in TEM. Journal of Applied Physics, 2011, 109, .	2.5	5
600	In Situ TEM Nanoindentation Studies on Stress-Induced Phase Transformations in Metallic Materials. Jom, 2016, 68, 226-234.	1.9	5
601	Terahertz transport dynamics in the metal-insulator transition of V 2 O 3 thin film. Optics Communications, 2017, 387, 385-389.	2.1	5
602	Controllable conduction and hidden phase transitions revealed via vertical strain. Applied Physics Letters, 2019, 114, 252901.	3.3	5
603	Pinning Efficiency of One-Dimensional Artificial Pinning Centers in YBa <sub>2</sub> Cu <sub>3</sub> O <sub>7-x</sub> Thin Films. IEEE Transactions on Applied Superconductivity, 2019, 29, 1-5.	1.7	5
604	Strain Effects on the Growth of La <sub>0.7</sub> Sr <sub>0.3</sub> MnO <sub>3</sub> (LSMO)–NiO Nanocomposite Thin Films via Substrate Control. ACS Omega, 2020, 5, 23793-23798.	3.5	5
605	Ultrafast, dry microwave superheating for the synthesis of an SbOx–GNP hybrid anode to investigate the Na-ion storage compatibility in ester and ether electrolytes. Chemical Communications, 2020, 56, 9663-9666.	4.1	5
606	Thermal stability of self-assembled ordered three-phase Au–BaTiO <sub>3</sub> –ZnO nanocomposite thin films <i>via in situ</i> heating in TEM. Nanoscale, 2020, 12, 23673-23681.	5.6	5
607	Effective doping control in Sm-doped BiFeO <sub>3</sub> thin films <i>via</i> deposition temperature. RSC Advances, 2020, 10, 40229-40233.	3.6	5
608	Dynamic tuning of dielectric permittivity in BaTiO <sub>3</sub> via electrical biasing. Materials Research Letters, 2020, 8, 321-327.	8.7	5
609	Tailorable multifunctionalities in ultrathin 2D Bi-based layered supercell structures. Nanoscale, 2021, 13, 16672-16679.	5.6	5
610	Thermal Stability of Nanocrystalline Gradient Inconel 718 Alloy. Crystals, 2021, 11, 53.	2.2	5
611	Ultrafast anchored SnO2 nanoparticles revealed capacity fade and hysteresis abated stable cycling performance for high-rate lithium-ion batteries. Carbon, 2021, 185, 608-618.	10.3	5
612	Epitaxial nanotwinned metals and alloys: synthesis-twin structure–property relations. CrystEngComm, 2021, 23, 6637-6649.	2.6	5

#	Article	IF	CITATIONS
613	Modeling of flash sintering of ionic ceramics. MRS Bulletin, 2021, 46, 67-75.	3.5	5
614	Achieving strong and stable nanocrystalline Al alloys through compositional design. Journal of Materials Research, 2022, 37, 183-207.	2.6	5
615	ZnO-AuxCu1â^'x Alloy and ZnO-AuxAl1â^'x Alloy Vertically Aligned Nanocomposites for Low-Loss Plasmonic Metamaterials. Molecules, 2022, 27, 1785.	3.8	5
616	A generalized 3D elastic model for nanoscale, self-assembled oxide-metal thin films with pillar-in-matrix configurations. Acta Materialia, 2022, 228, 117779.	7.9	5
617	Tribological behaviors of nanotwinned Al alloys. Applied Surface Science, 2022, 600, 154108.	6.1	5
618	TaN-TiN binary alloys and superlattices as diffusion barriers for copper interconnections. Journal of Electronic Materials, 2004, 33, L5-L5.	2.2	4
619	Role of columnar grain size in magnetization of La0.8MnO3 thin films grown by pulsed laser deposition. Applied Physics A: Materials Science and Processing, 2005, 81, 1423-1426.	2.3	4
620	Nanoporous Films and Nanostructure Arrays Created by Selective Dissolution of Waterâ€Soluble Materials. Advanced Science, 2018, 5, 1800851.	11.2	4
621	Tuning magnetic and optical properties through strain in epitaxial LaCrO3 thin films. Applied Physics Letters, 2021, 119, .	3.3	4
622	Integration of Self-Assembled BaZrO <sub>3</sub> -Co Vertically Aligned Nanocomposites on Mica Substrates toward Flexible Spintronics. Crystal Growth and Design, 2022, 22, 718-725.	3.0	4
623	Nanostructured DLC-Ag Composites for Biomedical Applications. Materials Research Society Symposia Proceedings, 2002, 750, 1.	0.1	3
624	The effect of growth rates on the microstructures of EuBa2Cu3O7â^'x films on SrTiO3 substrates. Applied Physics Letters, 2005, 86, 192508.	3.3	3
625	Comparative Study Between Similarly Processed \${m YBa}_{2}{m Cu}_{3}{m O}_{7-{m x}}\$ Films With \${m Y}_{2}{m BaCuO}_{5}\$ or \${m BaSnO}_{3}\$ Additions. IEEE Transactions on Applied Superconductivity, 2009, 19, 3152-3155.	1.7	3
626	Interlayer Effects on Oxygen Reduction Kinetics in Porous Electrodes of La0.5Sr0.5CoO3-l´. Journal of the Electrochemical Society, 2014, 161, F398-F404.	2.9	3
627	Grain growth of nanocrystalline 3C-SiC under Au ion irradiation at elevated temperatures. Journal Physics D: Applied Physics, 2016, 49, 035304.	2.8	3
628	Creating Ferromagnetic Insulating La <sub>0.9</sub> Ba <sub>0.1</sub> MnO <sub>3</sub> Thin Films by Tuning Lateral Coherence Length. ACS Applied Materials & Interfaces, 2021, 13, 8863-8870.	8.0	3
629	Ultrathin transparent Copper(I) oxide films grown by plasma-enhanced atomic layer deposition for Back-end-of-line p-Type transistors. Nano Express, 2021, 2, 020023.	2.4	3
630	Ellipsometry-based failure analysis on translucent LiMn0.5Ni0.3Co0.2O2 in half-cell thin-film lithium-ion battery on glass substrates. Materials Today Advances, 2021, 10, 100142.	5.2	3

#	Article	IF	CITATIONS
631	Recent Advances in Vertically Aligned Nanocomposites with Tunable Optical Anisotropy: Fundamentals and Beyond. Chemosensors, 2021, 9, 145.	3.6	3
632	Thermal Safety Analysis of Disordered Li-Rich Rock salt Li <sub>1.3</sub> Mn <sub>0.4</sub> Nb <sub>0.3</sub> O <sub>2</sub> Cathode. ACS Applied Energy Materials, 2022, 5, 516-523.	5.1	3
633	Optical dielectric properties of HfO2-based films. Journal of Vacuum Science and Technology A: Vacuum, Surfaces and Films, 2022, 40, .	2.1	3
634	TiN–Fe Vertically Aligned Nanocomposites Integrated on Silicon as a Multifunctional Platform toward Device Applications. Crystals, 2022, 12, 849.	2.2	3
635	Temperature dependent pinning efficiency in multilayer and single layer BZO/YBCO nanocomposite films. IOP Conference Series: Materials Science and Engineering, 2022, 1241, 012021.	0.6	3
636	Engineered reactive cosputtered SmxZr1–xOythin films as buffer layers for YBa2Cu3O7â^`Î′coated conductors. Journal of Materials Research, 2007, 22, 1082-1086.	2.6	2
637	Magnetotransport properties of epitaxial Pr0.5Ca0.5MnO3 films grown by a solution technique. Journal of Magnetism and Magnetic Materials, 2010, 322, 2708-2711.	2.3	2
638	Ferroelectric properties of epitaxial Bi3.15Nd0.85Ti3O12 films on SiO2/Si using biaxially oriented MgO as templates. Thin Solid Films, 2011, 519, 8023-8026.	1.8	2
639	Electrical and microstructural properties of N+ ion-implanted ZnO and ZnO:Ag thin films. Journal of Vacuum Science and Technology A: Vacuum, Surfaces and Films, 2011, 29, 03A108.	2.1	2
640	Tailoring radiation damage in ZnO by surface modification. Applied Surface Science, 2013, 276, 129-132.	6.1	2
641	Enhanced Flux Pinning Properties in \$hbox{YBa}_{2}hbox{Cu}_{3}hbox{O}_{7-delta}\$/ \$(hbox{CoFe}_{2}hbox{O}_{4})_{0.3}(hbox{CeO}_{2})_{0.7} \$ Multilayer Thin Films. IEEE Transactions on Applied Superconductivity, 2015, 25, 1-4.	1.7	2
642	Influences of Ag nanoparticles on the microstructure and texture of CeO2 films prepared by chemical solution deposition. Ceramics International, 2015, 41, 3197-3201.	4.8	2
643	Epitaxial growth and physical properties of ternary nitride thin films by polymer-assisted deposition. Applied Physics Letters, 2016, 109, 081907.	3.3	2
644	Thermal stability from calorimetric measurements of multilayered NiFe specimens with different layer thickness. Scripta Materialia, 2017, 137, 100-103.	5.2	2
645	Extrinsic size dependent plastic deformability of ZnS micropillars. Materials Science & Engineering A: Structural Materials: Properties, Microstructure and Processing, 2020, 792, 139706.	5.6	2
646	Linking far-from-equilibrium defect structures in ceramics to electromagnetic driving forces. Journal of Materials Chemistry A, 2021, 9, 8425-8434.	10.3	2
647	Hybrid Ag–LiNbO3 nanocomposite thin films with tailorable optical properties. Nanoscale Advances, 2021, 3, 1121-1126.	4.6	2
648	Mechanical and Electrical Properties of Nanocrystalline and Epitaxial TiN Films. Materials Research Society Symposia Proceedings, 2001, 697, 841.	0.1	1

#	Article	IF	CITATIONS
649	Microstructures and Mechanical Properties of Nanostructured Copper-304 Stainless Steel Multilayers Synthesized by Magnetron Sputtering. Materials Research Society Symposia Proceedings, 2002, 740, 1.	0.1	1
650	Studies on Epitaxial Relationship and Interface Structure of AlN/Si(111) and GaN/Si(111) Heterostructures. Materials Research Society Symposia Proceedings, 2002, 743, L3.24.1.	0.1	1
651	Growth of TiN/AIN Superlattice by Pulsed Laser Deposition. Materials Research Society Symposia Proceedings, 2002, 750, 1.	0.1	1
652	Microstructural Study of <tex>\$rm EuBa_2rm Cu_3rm O_7\$</tex> Films by High Resolution X-ray Diffraction. IEEE Transactions on Applied Superconductivity, 2005, 15, 2731-2734.	1.7	1
653	Materials science challenges for high-temperature superconducting wire. , 2010, , 299-310. Optimizing Flux Pinning of <inline-formula> <tex-math< td=""><td></td><td>1</td></tex-math<></inline-formula>		1
654	notation="TeX">\$hbox{YBa}_{2}hbox{Cu}_{3}hbox{m O}_{7hbox{-}{delta}} \$ (YBCO) Thin Films With Unique Large Nanoparticle Size and High Concentration of <inline-formula> <tex-math notation="TeX">\$hbox{m Y}_{2}hbox{BaCuO}_{5}\$</tex-math></inline-formula> (Y211) Additions. IEEE Transactions on Applied	1.7	1
655	Superconductivity 2015, 25, 1-5, 1-5, Ramifications of Pulsed Laser Deposition Growth Temperature on BaHfO <sub>3</sub> and Y <sub>2</sub> O <sub>3</sub> Doped Y-Ba-Cu-O Thin Films' Microstructure and Performance. IEEE Transactions on Applied Superconductivity, 2021, 31, 1-5.	1.7	1
656	Low voltage control of magnetism in BaFe10.2Sc1.8O19/BaTiO3 bilayer epitaxial thin film at temperatures up to 390 K. Applied Physics Letters, 2022, 120, 062401.	3.3	1
657	Single Crystal TaN Thin Films on TiN/Si Heterostructure. Materials Research Society Symposia Proceedings, 2002, 716, 881.	0.1	0
658	Copper Diffusion Characteristics in Single Crystal and Polycrystalline TaN. Materials Research Society Symposia Proceedings, 2002, 745, 6111.	0.1	0
659	Effects of Eu interfacial mobility on the growth of epitaxial EuBa2Cu3O7â^1̂ films. Applied Physics Letters, 2005, 86, 101912.	3.3	0
660	Comparison of Different Routes for Improving Vortex Pinning in YBa2Cu3O7 Thin Films and Coated Conductors. AIP Conference Proceedings, 2006, , .	0.4	0
661	Low resistivity hafnium nitride thin films as diffusion barriers for Cu interconnects. , 2007, , .		0
662	Tunable dielectric properties of lead strontium titanate thin films by sol-gel technique. , 2008, , .		0
663	Spontaneous ordering, strain control and mutlifunctionality in vertical nanocomposite heteroepitaxial films. , 2008, , .		0
664	Strongly enhanced current densities in superconducting coated conductors of YBa2Cu3O7â^'x + BaZrO3. , 2010, , 327-331.		0
665	MICROSTRUCTURE AND CRITICAL CURRENT DENSITY OF YBa[sub 2]Cu[sub 3]O[sub 7â^X]+BaSnO[sub 3] THICK FILMS GROWN WITH PRE-MIXED PULSED LASER ABLATION TARGET. , 2010, , .		0
666	SECOND PHASE (BaGeO[sub 3], BaSiO[sub 3]) NANOCOLUMNS IN YBa[sub 2]Cu[sub 3]O[sub 7â^'x] FILMS. ,		0

666 2010, , .

#	Article	IF	CITATIONS
667	Atomic-scale EDS Mapping for Chemical Imaging and Quantification of Interdiffusion in Self-assembled Vertically Aligned Nanocomposite Thin Films. Microscopy and Microanalysis, 2015, 21, 2249-2250.	0.4	0
668	Ferroelectric thin films and nanostructures: current and future. , 2019, , 19-39.		0
669	Reducing Leakage Current and Enhancing Polarization in Multiferroic 3D Super-nanocomposites by Microstructure Engineering. Nanotechnology, 2022, , .	2.6	0
670	Interface Engineering for Enhanced Magnetic Vortex Pinning by 1D-BZO APCs in a Wide Angular Range. IOP Conference Series: Materials Science and Engineering, 2022, 1241, 012022.	0.6	0